CATALYST CHALLENGES ON THE ROAD TO THE HDYROGEN ECONOMY

Thomas A Giroux

Engelhard Corporation
101 Wood Avenue, Iselin, NJ 08830

Overview

The ideal goal for hydrogen production would be derived from solar, wind or other renewable, natural sources of energy. The primary driving force is the decreased dependence on liquid petroleum with the positive consequence of elimination of primary pollutants and reduced green house gas emissions. It is not expected that these sources of energy will be available soon. Reforming of hydrocarbons and alcohols will be the primary source of hydrogen as a transitional solution.

The applications for hydrogen generation vary widely in scale, scope, and their demands on catalysis. Microreactors intended to power small portable devices such as a cell phone push the limits of coating technology. Manufacturers are looking to advances in catalyst activity to shrink hydrogen generators to the point where they could be mounted on the walls of a garage at home to refuel cars, feed fuel cells, and use captive energy for hot water for home heating. Developers of future distributed residential power suppliers want catalysts flexible enough to work with various fuels such as kerosene, natural gas, and LPG to make standalone hydrogen generators to power 1-5 kW fuel cells and cogeneration systems to redefine the electricity distribution infrastructure. Industrial users want reliable, durable, economic catalysts to help replace their bottle gas deliveries with process-critical moderate sized hydrogen generation skids to feed their metal processing, hydrogenation, and cooling needs. Even on the large scale, centralized hydrogen producers are looking at ways to debottleneck existing capital investments by taking advantage of new catalyst developments to boost productivity and throughput. Momentum continues to build as new processes and applications for distributed generation of hydrogen are being developed worldwide and present us with a spectrum of challenges and opportunities for catalyst product and technology developments.

We believe precious metals supported on ceramic monoliths, metal monoliths, and other high-geometry surfaces such as heat exchangers are the technologies for future generations of such hydrogen generation systems. These catalysts are durable against the daily start/stop cycles experienced in operations. The highly active catalyst washcoat deposited on the walls of monolithic structures can permit decreases of more than 10 times the size of the traditional base metal catalyst reformer. They offer greater structural stability, more rapid response to transient operation and lower pressure drop than pelletized catalysts. These properties contribute to a robust, reliable and durable reformer system capable of meeting the lifetime requirement for economical hydrogen generation systems especially when precious metal recycle is considered in the lifecycle cost of the system.

The talk will provide an overview of some of the critical catalytic issues that must be overcome in order to see the commercialization of distributed hydrogen generation. Included will be the limitations of traditional base metal catalysts for hydrogen generation and how precious monolithic catalysts circumvent many of these issues to provide a viable solution.

STRATIFIED CATALYSTS FOR METHANE PARTIAL OXIDATION

Gisele Tong, Julie Flynn, & Corey Leclerc

Department of Chemical Engineering
McGill University
3610 University St
Montréal, Québec H3A 2B2 CANADA

Introduction

Catalytic partial oxidation (CPO) is a viable process for the production of hydrogen for fuel cells. CPO is characterized by small residence times on the order of 1-10 ms and is exothermic, so once the catalyst lights off it remains catalytically active without heat input. The CPO catalyst has a small thermal mass, so it can be started in seconds[1,2]. The reactor is quite robust in that it can be used to convert methane[3], ethanol[4], gasoline[5], and diesel[6]. The short residence time and auto-thermal behavior make CPO ideal for small, hydrogen fuelled systems.

Catalysts design and selection for CPO has received much attention from the academic community. Many catalysts are active for CPO, but rhodium has been found to obtain the highest fuel conversions and highest hydrogen selectivities with the most stable operation[7]. Unfortunately, rhodium is expensive. In addition, rhodium pricing over the past two decades has not been stable with large spikes in pricing around 1990 and 2000.

The CPO process requires half a mole of oxygen per mole of methane.

$$CH_4 + \tfrac{1}{2} O_2 \rightarrow 2 H_2 + CO \qquad \Delta H = -36 \text{ kJ/mol}$$

Researchers have shown that, for methane, the CPO process takes place in two sequential steps[8,9]. The first step is a complete oxidation of one-quarter of the methane to use up all of the oxygen.

$$CH_4 + 2 O_2 \rightarrow 2 H_2O + CO_2 \qquad \Delta H = -802 \text{ kJ/mol}$$

The second step is reforming of the remaining methane by water and carbon dioxide.

$$CH_4 + H_2O \rightarrow 3 H_2 + CO \qquad \Delta H = 206 \text{ kJ/mol}$$
$$CH_4 + CO_2 \rightarrow 2 H_2 + 2 CO \qquad \Delta H = 247 \text{ kJ/mol}$$

The first, highly exothermic step supplies the heat to the endothermic reforming reactions.

In this work, catalysts were chosen based on the two step process. Instead of trying to optimize one metal to carry out both steps of the process, two metals were chosen, one to optimize the first step and the other to optimize the second step. The millisecond process is ideal for a stratified catalyst; the high space velocities lead to large amounts of heat convected from the exothermic step to the endothermic step, thus increasing the yield of hydrogen. In addition, rhodium is not used in the catalyst, so the price of the catalyst can be reduced by over 50% depending on the metal combination.

Experimental

The reactions are carried out in a quartz tube of 18 mm in diameter. Methane and air are fed to the reactor by mass flow controllers and are premixed up stream of the catalyst. The foam catalyst is wrapped in alumino-silicate paper to prevent gas bypass around the catalytic foam. Blank foams are placed immediately upstream and downstream from the catalytic foam to prevent the loss of heat due to radiation. A K-type thermocouple was placed through the downstream heat shield to make intimate contact with the back face of the catalyst. All temperature data shown come from the measurements of this thermocouple. In the case of stratified catalysts, two foams were placed in the reactor sequentially with the combustion catalyst upstream of the reforming catalyst. For comparison, experiments were carried out with pure rhodium and pure platinum catalysts as well. For these catalysts, a single foam was used that had the same axial dimensions as the two stratified catalysts combined. In addition, experiments were carried out with the reforming catalyst upstream of the combustion catalyst to assure that the order of the catalysts was important. **Figure 1** shows the reactor setup and a comparison of stratified versus single bed catalysts.

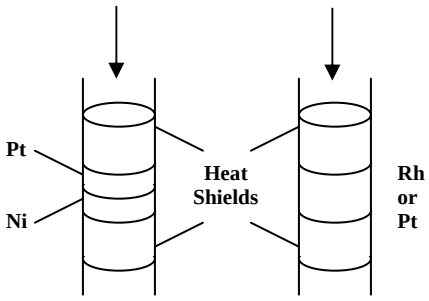

Figure 1. The stratified and single component reactor set-ups

Catalysts were made by first wash coating an 80 pores per inch, 17 mm diameter α-alumina foam monolith with a γ-alumina washcoat. After washcoating, a solution of metal salt was dripped onto the foam. The foam was then air dried and then calcined in air at varying temperatures and times depending on the metal. In this work, platinum, from hexachloroplatinic acid, nickel, from nickel (II) nitrate, and rhodium, from rhodium (II) nitrate, were used in this study. For all catalysts, metal loadings were typically between 4 and 5% by weight.

Gases leaving the reactor were separated and analyzed by gas chromatography. An HP-PLOT molesieve 5A column was used to separate methane, oxygen, nitrogen, and carbon monoxide, while a HP-PLOT Q capillary column separated carbon dioxide from the other gases. The gases were analyzed on a thermal conductivity detector. Carbon balances closed to within ±5%.

Results and Discussion

Stratified catalysts were compared to single component catalysts for varying feed stoichiometries. In these experiments, the methane oxygen ratio was varied between 1.7 and 2.1; 2.0 is the exact stoichiometry for the partial oxidation reaction. The stratified catalysts included a platinum (combustion) foam followed by a nickel (reforming) foam (Pt/Ni). This second catalyst was the reverse of the first one, with the nickel catalyst leading the combustion catalyst (Ni/Pt). The two single component catalysts were made up of rhodium or platinum.

Figure 2a shows the back face temperature of the catalyst for four different catalysts. All catalysts show a gradual decrease in back face temperature as the methane to oxygen ratio increases. Of particular importance is the temperature of the Ni/Pt catalyst. This catalyst experienced back face temperature significantly higher than the other three catalysts. Ideally, this process will be carried out at as low a temperature as possible, which does not favor the Ni/Pt catalyst.

Figure 2b shows the methane conversion with varying feed ratios. Again, all catalysts show a decrease in methane conversion as

the methane to oxygen ratio increases. The Pt/Ni catalyst performs as well or better than the rhodium catalyst. At higher ratios, the improvement of the Pt/Ni catalyst is significantly higher than the Rh catalyst. The Ni/Pt catalyst performs quite well, while the Pt catalyst does not perform as well especially at higher ratios.

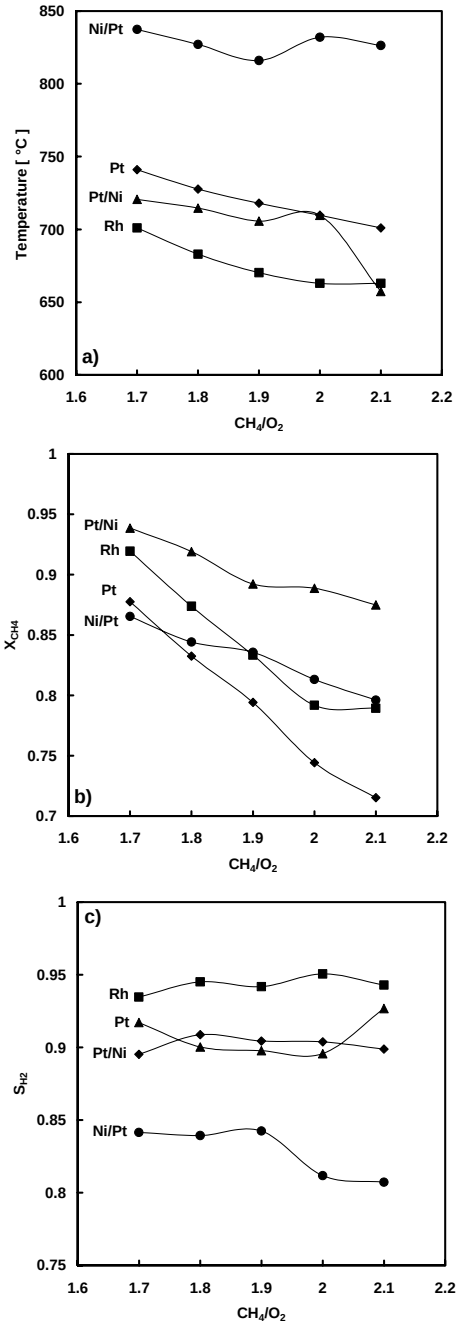

Figure 2. Results of experiments in which the feed ratio of methane to oxygen was varied for a) temperature, b) methane conversion, and c) hydrogen selectivity.

Figure 2c shows the hydrogen selectivity as a function of methane to oxygen ratio. Rhodium shows the highest selectivity to hydrogen. However, it is not much higher than the selectivities obtained from platinum or Pt/Ni. The Ni/Pt catalyst has the lowest selectivity of the four catalysts.

Figure 3 shows the temperature, conversion, and selectivities for a 10 hour long experiment. Since nickel is known to deactivate under these feed conditions, it was necessary to test the stability of the Pt/Ni catalyst. For all measurements, there was no reduction in performance for the Pt/Ni catalyst, indicating that it is stable over the 10 operating period.

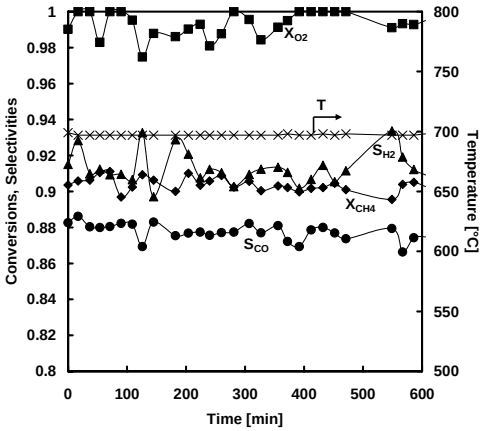

Figure 3. 10 hour experiment to determine Pt/Ni catalyst stability

Conclusions

A Pt/Ni stratified catalyst has obtained hydrogen yields that are comparable to rhodium, the best catalyst available for methane partial oxidation, over a wide range of operating conditions. It was shown that the order of the stratified catalysts is important. The catalyst was also shown to be stable over a 10 hour period despite the potential for deactivation.

Acknowledgements. Gisele Tong would like to thank the Natural Science and Engineering Research Council of Canada for financial support through the Undergraduate Student Research Awards. Julie Flynn would like to thank the Eugenie Ulmer Lamothe Scholarship Fund for financial Support. Corey Leclerc would like to thank Dr. Karthik Venkataraman for valuable discussions regarding the research.

References

(1) Leclerc, C. A.; Redenius, J. M.; and Schmidt, L. D. *Cat. Lett.***2002**, 79, 39.
(2) Williams, K. A.; Leclerc, C. A.; and Schmidt, L. D. *AIChE J.* **2005**, 51, 247.
(3) Hickman, D. A.; and Schmidt, L. D. *Sci.* **1993**, 259, 343.
(4) Deluga, G. A.; Salge, J. R. ; Schmidt, L. D. ; and Verykios, X. E. *Sci.*, **2004**, 303, 993.
(5) O'Connor, R. P.; Klein, E. J.; and Schmidt, L. D. *Cat. Lett.* **2000**, 70, 99.
(6) Krummenacher, J. J.; West, K. N.; and Schmidt, L. D. *J. Cat.* **2003**, 215, 332.
(7) Torniainen, P. M.; Chu, X.; and Schmidt, L. D. *J. Cat.* **1994**, 146, 1.
(8) Buyevskaya, O.V.; Wolf, D.; and Baerns, M. *Cat. Lett.* **1994**, 29, 249.
(9) Mallens, E. P. J.; Hoebink, J. H. B. J., and Marin, G. B. *J. Cat.* **1997**, 167, 43.

STEAM REFORMING CATALYSTS FOR MICROCHANNEL REACTOR

Junko M. Watson and Frank P. Daly

Velocys, Inc.
7950 Corporate Blvd.
Plain City, OH 43064

Introduction

Velocys Inc. has developed a microchannel processing system for hydrogen production by steam reforming of methane (SMR). The catalyst used for this system is Rh supported on alumina. Previously, Wang *et al* reported the use of Rh supported on spinel for SMR at short contact times [1, 2]. The effect of Mg, Ba, La, Pr and Y addition and pre-aging conditions on alumina stabilization under SMR conditions has been studied. Catalyst loading as well as coating methodology, key variables for microchannel devices, has also been studied. Catalyst performance was tested in a single microchannel device at 15 - 30 atm, 3:1 steam to carbon ratio, 3-6 milliseconds contact time, and temperature of 840 ^{o}C. Rh supported on hydrothermally pre-aged Mg/Al_2O_3 showed excellent durability over a period of 2,500 hours time on stream. Catalyst characterization including N_2 BET surface area, hydrogen chemisorption, XRD, TEM, and SEM was also performed.

Experimental

Catalyst Synthesis and Characterization. Catalysts were prepared via incipient wetness technique. The alumina precursor was alumina sol (Dispal 18N4-80, Sasol). The dopant precursors included lanthanum nitrate, barium nitrate, yttrium nitrate, praseodymium nitrate, and magnesium nitrate (Aldrich). Rhodium nitrate (Engelhard) was used as the Rh precursor. The alumina precursor was converted to aluminum oxide by calcining in air at 450^{o}C for 4 hours. The calcined alumina was then impregnated with magnesium nitrate and further calcined at 1000 ^{o}C for 4 hours. Thermal aging was performed at 1050 ^{o}C for 100 hours in air. Hydrothermal aging was carried out at 92 5^{o}C for 100 hours in 66% steam at steam partial pressures in the range of 0.6 – 17 atm.

Rh dispersion was measured by static volumetric H_2 chemisorption methods at 25 ^{o}C using ASAP 2010 (Micromeritics). BET surface area was also measured using ASAP 2010. TEM analysis was conducted on a JEOL 2010 high-resolution analytical electron microscope operating at 200 kV with a LaB_6 filament. TEM analysis was performed at the Pacific Northwest National Laboratory.

Testing Apparatus. Reaction experiments were conducted in a microchannel flow reactor made of alloy 617. The microchannel reactor (2" long rod with 0.5" DI) was EDM wire cut to create a slot sized at 0.16" x 2" x 0.01". A FeCrAlY fin was used as catalyst substrate after heat treatment at 900 ^{o}C for 8 hours in air. The catalyst is washcoated onto the substrate and inserted into the reactor slot. Reactor wall temperature was measured by a type K thermocouple which is inserted in a thermal well. The temperature was measured 0.03" away from the back side of the FeCrAlY insert. Catalyst is first reduced at 450 ^{o}C with 10 % H_2 in He for 2 hours. The SMR reaction conditions were 3:1 steam:carbon ratio, 3.0 – 6.0 millisecond contact time, 15 - 27 atm pressure, 800 – 900 ^{o}C reaction temperature.

Gases were controlled by Brooks 5850E mass flow controllers and water was fed using an Accuflow Series III HPLC pump. Gas composition was measured by micro GC 3000A (Agilent).

Results and Discussion

Figures 1 and 2 are lifetime test results at a 3:1 steam:carbon ratio, 4.5 ms contact time, 15 atm pressure and 850 ^{o}C reactor wall temperature for $Rh/La\text{-}Al_2O_3$ (thermally pre-aged) and $Rh/Mg\text{-}Al_2O_3$ (hydrothermally pre-aged), respectively. Test results were obtained using a single microchannel reactor containing a FeCrAlY fin coated with a catalyst having a rhodium oxide loading of 1.3 mg/in^2. The La/Al_2O_3 support was thermally pre-aged at 1050 ^{o}C for 100 hours in air at 1atm and the Mg/Al_2O_3 support was hydrothermal pre-aged at 925 ^{o}C for 100 hours in 66% steam at 25 atm. Measured surface areas of the supports are presented in Table 1. Under thermal pre-aging conditions, the La-stabilized alumina had a 6-fold higher surface area than the Mg-stabilized support (Figure 3); however, under hydrothermal pre-aging conditions, the Mg-stabilized support had a 3-fold higher surface area than the La-stabilized support.

For the thermally pre-aged $Rh/La\text{-}Al_2O_3$ catalyst, a continual decline in methane conversion was observed within 700 hours on stream (Figure 1). A thermally pre-aged $Rh/Mg\text{-}Al_2O_3$ catalyst displayed a similar trend in deactivation under the same conditions. However, when Rh was supported on hydrothermally pre-aged Mg/Al_2O_3, the SMR activity was steady for over 2500 hours (Figure 2). As displayed in Figure 2 the contact time was switched from 4.5 ms to 3.0 ms to move from equilibrium limited to kinetically limited conditions. For the next 1000 hours, no catalyst deactivation was observed.

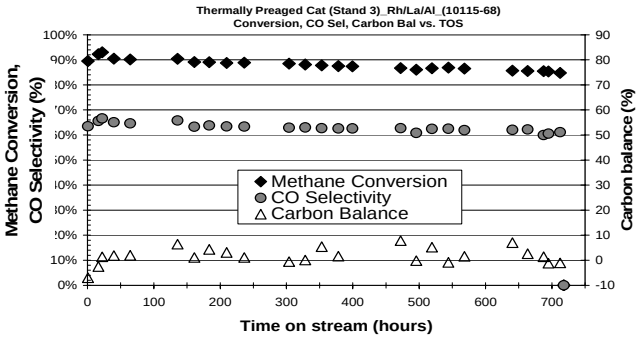

Figure 1. Thermally pre-aged $Rh/La\text{-}Al_2O_3$ catalyst performance (25 mg/in^2 total catalyst loading, 5 wt% Rh_2O_3)

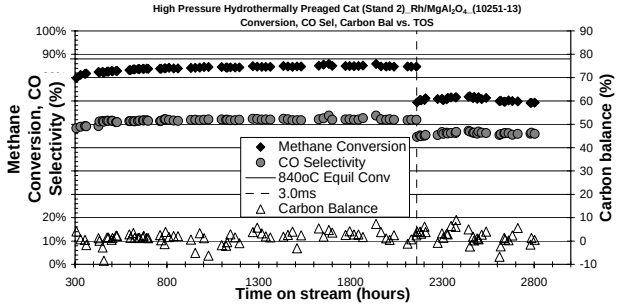

Figure 2. Hydrothermally pre-aged $Rh/Mg\text{-}Al_2O_3$ catalyst performance (13.6 mg/in^2 total catalyst loading, 9.3 wt% Rh_2O_3)

Table 1. BET Surface Area

	Fresh (m^2/g)	1 atm Thermal (1000°C, air, 100hrs) (m^2/g)	1atm Hydrothermal (66% steam, 925°C, 100hrs) (m^2/g)	25atm Hydrothermal (66% steam, 925°C, 100hrs) (m^2/g)
3%La/Al_2O_3	105.3	79.5	59.3	3.3
6%Mg/Al_2O_3	81.9	12.2	46.2	6.4

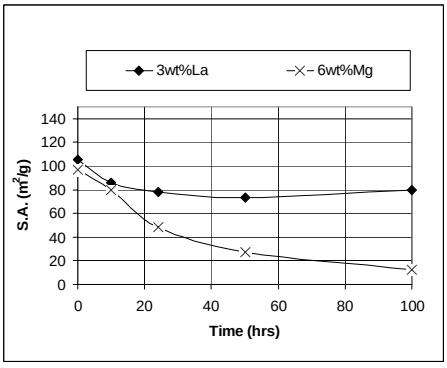

Figure 3. BET surface area with aging time on stream at 1000 °C in air.

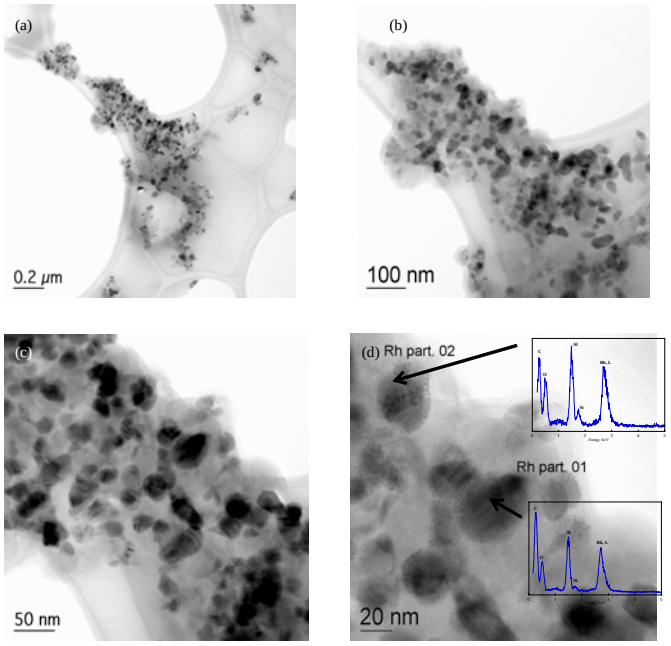

Figures 4 (a-d). TEM bright field micrographs of fresh Rh/La-Al_2O_3 (Specimen 10115-40)

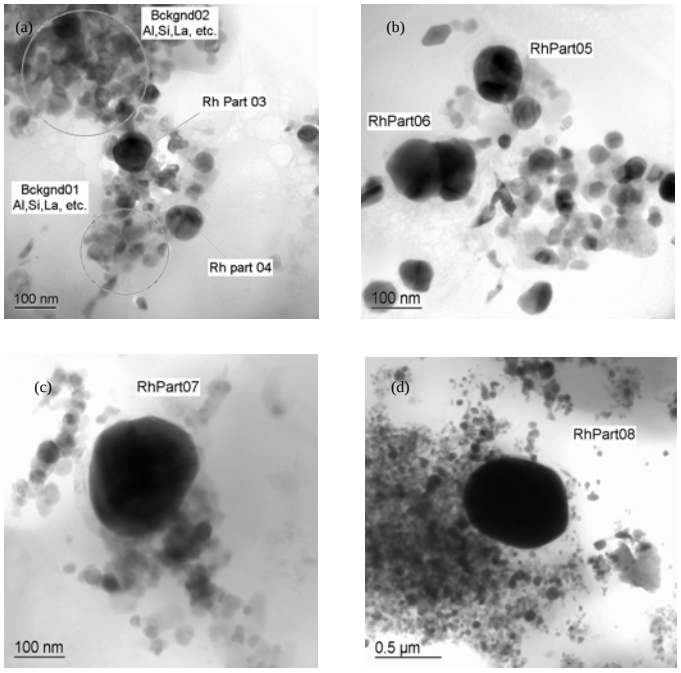

Figures 5 (a-d). TEM bright field micrographs of spent Rh/La-Al_2O_3 which was on stream for 1600 hours at 3 to 1 steam to carbon, 3.0 - 4.5 ms contact time, and highest wall temperature of 950 °C. (Specimen 10115-33)

Bright field micrographs of fresh Rh/La/Al_2O_3 catalyst (10115-40) are shown in **Figures 4** (a-d). 5.3 mg of the catalyst was coated on a FeCrAlY substrate. Rh loading was 24wt%. The dark particles were identified as Rh by EDS analysis and their sizes ranged from ~20 – 50 nm in diameter. **Figures 5** (a-d) are also bright field micrographs of spent Rh/La-Al_2O_3 which was on stream for 1600 hours under 3 to 1 steam to carbon ratio, 3.0 - 4.5 ms contact time, and the maximum wall temperature of 950 °C. Conversion and selectivity profiles of this sample also showed a continual decline similar to Figure 1. The range of Rh particle sizes on the spent sample, which consisted of 7.3 mg of catalyst with 21 wt% rhodium loading, was ~90 – 700 nm. The crystallite size has grown at least 3-fold and as much as 35-fold. This indicates that severe metal sintering was observed on the deactivated catalyst.

References

1. Wang, Y., Tonkovich, A.L.Y., VanderWiel, D.P. U.S. Patent No. 6,607,678, **2003**
2. Wang, Y., Chin, Y.H., Rozmiarek, R.T., Johnson, B.R., Gao, Y., Watson, J., Tonkovich, A.L.Y., VanderWiel, D.P. *Cat. Today* 2004, 98, 575-581.

HYDROGEN PRODUCTION BY CATALYTIC DECOMPOSITION OF METHANE OVER Ni AND Ni-Cu BASED CATALYSTS

I. Suelves[a], M.J. Lázaro[a], R. Moliner[a], Y. Echegoyen[a], J.M.Palacios[b]

[a] Instituto de Carboquímica CSIC, Miguel Luesma Castán, 4. 50015-Zaragoza
[b] Instituto de Catálisis y Petroleoquimica CSIC, Campus UAM, 28049-Madrid, Spain

Introduction

The social concern generated by presumable climate changes derived from the emission of greenhouse gases, in particular CO_2, will force in the near future the adoption of energetic policies promoting the progressive reduction of CO_2 emissions. Among them, utilisation of hydrogen as energy carrier, instead of usual liquid hydrocarbons, by the increasing use of fuel cells, instead of the traditional IC engines, is one of the most promising technologies proposed. [1]

It is generally accepted that in the near-to-medium terms, hydrogen production will continue relying on fossil fuels, primarily natural gas. [2]. Nowadays, among the different technologies used for large scale hydrogen production, steam reforming of natural gas, SMR, is one most widely used. However, this process involves the emission of CO_2, unless it is captured and stored what increase the cost of hydrogen production around 20-50% [2]. An alternative process to SMR is the thermocatalytic decomposition, TCD, of natural gas through the production of CO-free hydrogen and pure carbon as a reaction product of significant added value. TCD, however, still needs the knowledge of several scientific aspects, in particular, the different operating mechanism of reaction to select the most suitable catalysts and optimisation of the operating conditions.

In our previous work [3], TCD of methane using a commercial Ni catalyst it was proved the achievement of hydrogen yields close to the thermodynamic values. It was also shown that the time for catalyst deactivation depends on the operating conditions, so that, the higher the methane flow rate the shorter the catalyst life. The deposited carbon appears either as long filaments a few nanometres in diameter emerging from Ni particles or as uniform coatings on these particles. Operating conditions promoting high decomposition rates enhance the formation of uniform coating versus long filaments shortening the catalyst life. In this work, Ni and Ni-Cu catalyst were prepared in order to evaluate the influence of the amount of nickel in the samples and the presence of copper as a promoter on methane conversion, catalyst life and quality of the carbon produced.

Experimental

Catalysts. Catalysts with different Ni/Al and Ni/Cu/Al ratio were prepared by co-precipitation from an aqueous solution of the respective nitrates with sodium carbonates following the procedures described in literature [4]. The precipitates were then washed, dried and calcined at 450ºC.

A commercial catalyst composed of 65 wt% of Ni supported in a mixture of silica and alumina has been also used for comparison.

Activity tests. Prior to activity tests, all catalysts were subjected to a reduction treatment using a flow of pure hydrogen of 20 ml/min for 3h. Different reduction temperatures (550-650ºC) have been tested to evaluate the influence of the pre-reduction treatment on the catalyst behaviour and especially on the purity of the hydrogen produced.

Activity tests were run in a laboratory fixed bed quartz reactor 2 cm i.d., 60 cm height, using pure CH_4 as feeding gas at different reaction temperatures (700-800ºC). The outlet gas composition from the reactor was analyzed by gas chromatography using two packed columns and TCD detector. The evolution of CO and CO_2 has been followed by a gas chromatograph equipped with a flame ionization detector, modified with connection of two packed columns to a catalytic hydrogenation reactor. This way, levels of carbon oxides in the range of ppmv can also be measured.

Characterization techniques. The textural properties of the fresh and used samples were measured by N_2 adsorption at 77 K. The homogeneity, degree of Ni dispersion in the fresh catalysts and the study of the morphological appearance of the deposited carbon have been carried out in a scanning electron microscope (SEM). Powder X-ray diffraction (XRD) patterns for the study of the crystalline chemical species and transmission electron microscopy (TEM) studies have been also carried out.

Results and discussion

TCD of methane using Ni or Ni:Cu catalyst proceeds with hydrogen yields close to the thermodynamic values.
Figure 1 show some of the results obtained for the prepared catalysts and the comparison with the commercial catalyst used in our previous work [2]. The co-precipitation catalysts show a similar behaviour to the commercial one, even better when a small concentration of copper is introduced in its composition.

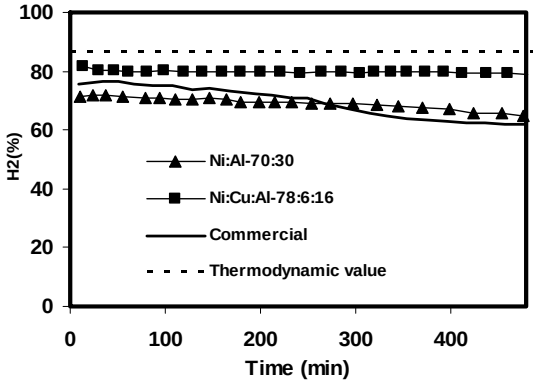

Figure 1. Hydrogen production (%vol) T: 700ºC- Methane flow:20 ml/min

Table 1 shows the initial, r_o, and the long term, rf, methane decomposition rates, and the carbon to catalyst weight ratio, Rw, for some selected samples.

No important differences in behaviour were found when the percentage of nickel on the samples was varied between 70-90%. Nickel percentages below 30% result in a low initial methane conversion. As shown in figure 1, the introduction of a small amount of copper increases both the initial and the long term decomposition rates of the catalyst but excessive copper concentrations (25%) results in lower methane conversions. It seems that copper is not, in fact, an active catalyst of the TCD of methane but a promoter acting through the isolation of Ni sites in the Ni lattice by partial cation replacement.

Table 1. Initial activity, final activity and accumulated carbon (T: 700ºC; Flow: 20ml/min; Time: 8h)

Ni:Cu:Al	r_0 (mmol/min.g)	r_f (mmol/min.g)	Rw
Comercial	1.9	1.6	9.1
70:-:30	1.7	1.5	8.5
90:-:10	1.8	1.5	9.2
25:-:75	0.7	0.1	3.0
75:2:23	1.8	1.6	10.2
78:6:16	2.0	1.8	10.7
50:25:25	1.5	1.5	8.9

At 700ºC the catalysts activity does not decay after 8 h on-stream (except for the catalyst with a percentage of nickel below 30%) and a weight ratio of carbon to nickel between eight and eleven was obtained without catalyst deactivation. When temperature was increased up to 800ºC a fast depletion of activity was observed for both Ni and Ni:Cu catalysts.

Regarding the purity of the hydrogen obtained, CO evolved decreases when pre-reduction temperature increases and when a small amount of Cu is introduced in the fresh catalysts. The presence of Cu also enhances the reduction of Ni species present as mixed oxides in samples after calcination, lowering its reduction temperature. The presence of NiO results in lower CH_4 conversions and also in a higher CO evolution whose presence is undesirable for further hydrogen use in low- temperature fuel cells.

Carbon characterization

The specific surface areas (not shown) of the still active catalyst are lower than that of the fresh catalyst, due to the presence of deposited carbon. However this deposited carbon must present some porosity since it is the dominant component in the samples at the end of the tests.

SEM examination of the deposited carbon shows that it appears as long filaments a few nanometres in diameter emerging from Ni particles coexisting with uniform coatings on the Ni particles. Although the relative concentration of these two carbon forms cannot be achieved, a simple examination of the respective SEM images evidences that long filaments are more abundant than uniform coatings for all catalysts tested at 700ºC. When the reaction temperature is increased up to 800ºC the morphology of the deposited carbon changes, appearing mainly as uniform coatings on Ni particles shortening the catalyst life.

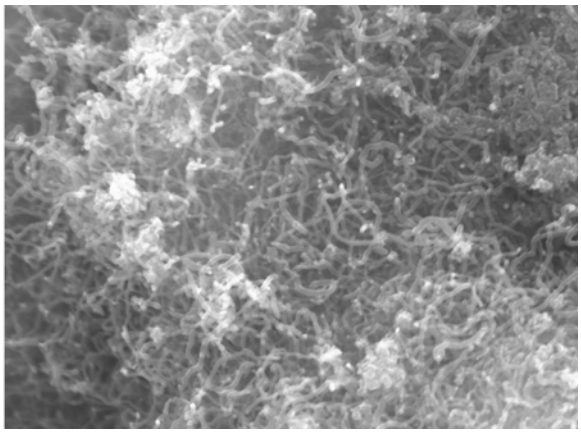

Figure 2. SEM micrograph of a still active sample (Co-precipitation catalyst Ni:Cu:Al-78:6:16.T:700ºC- Methane flow rate:20 ml/min)

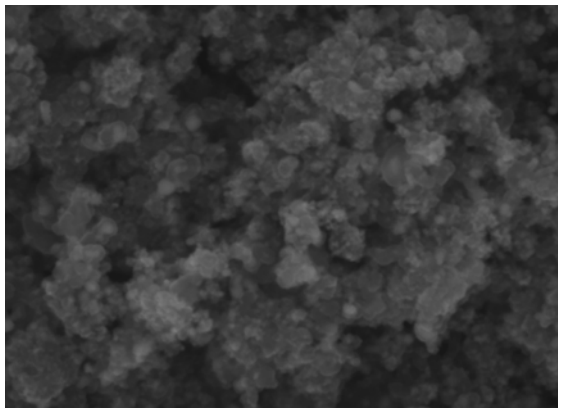

Figure 3. SEM micrograph of a deactivated sample (Co-precipitation catalyst Ni:Cu:Al-78:6:16. T:800ºC- Methane flow rate:20 ml/min)

Acknowledgement. This work has been supported with funds provided by the Spanish Ministery of Science and Technology. Research Project PPQ2002-03346 and by the Aragon Government by means of the recognition as Consolidated Research Group.

References

1. Green Book of Energy for Europe. European Commission. Brussels.November, 29. **2000**

2. Hart D., Freud P., and Smith A. Hydrogen Today and Tomorrow. IEA GHG Programme. April **1999.** ISBN 1 898373248

3. I.Suelves, M.J. Lázaro, R. Moliner, B.M. Corbella and J.M. Palacios. International Journal of Hydrogen Energy, in press

4. M.A. Ermakova, D. Yu. Ermakov, G.G. Kuvshinov. Applied Catalysis A: General 201, 61-70, **2000**

5. M.A. Ermakova, D. Yu. Ermakov, G.G. Kuvshinov and L.M. Plyasova. Jounal of Catalysis 187,) 77-84, **1999.**

DEACTIVATION KINETICS DURING THE STEAM REFORMING OF DIESEL- FUEL COMPONENTS

Sandeep K. Goud and Martin A. Abraham[*]

Dept of Chemical and Environmental Engineering
University of Toledo, Toledo OH 43606

William A. Whittenberger
Catacel Corp.
Garrettsville, OH

Introduction

The recent discussion regarding the coming hydrogen economy has provided unique opportunities to investigate available technologies for the delivery of hydrogen. Current fuel distribution systems are based on hydrocarbon fuels, such as diesel and natural gas, not hydrogen. Therefore, wide spread use of fuel cells will require development of a hydrogen distribution infrastructure or an efficient process to produce hydrogen from hydrocarbon fuels. Hydrogen generation from existing resources, such as natural gas, gasoline and diesel fuel, is a viable alternative for the near-term.

For the conversion of distillate fuels, such as diesel or jet fuel, the presence of sulfur-containing compounds leads to rapid deactivation of the catalyst. Development of a sulfur-tolerant catalyst would represent an important technical advance; for example, InnovaTek claims a sulfur-tolerant (up to 100 ppm S) reforming catalyst for conversion of diesel fuel that operates at a steam to carbon ratio of 3.6 for 220 hr with no deactivation [[i]]. Much of the recent desulfurization research has concentrated on ZnO-based sorbents for sulfur removal since the thermodynamics of ZnO-H_2S reaction is very favorable [[ii], [iii]]. In addition, the sulfur capacity of ZnO (g S/g ZnO) is very high (~0.39 g S/ g ZnO).

This paper describes our efforts to understand the performance of a Pd based monolith catalyst in the steam reforming of n-hexadecane (as a surrogate for diesel fuel) for the production of hydrogen. The present study describes the effect of steam to carbon ratio (S/C), temperature (T) and sulfur content (S) on the deactivation of the catalyst. A statistical analysis of the experiments has been completed to determine the combined effect of these three parameters on the rate of catalyst deactivation. Novel catalysts in which base metal oxides have been incorporated into the washcoat have also been evaluated for deactivation, and shown to provide superior sulfur tolerance. A second statistically designed experiment has been used to evaluate the performance of the catalyst at various loadings of base metal oxide additive.

Experimental

At the University of Toledo, steam reforming of n-hexadecane, used as a simulant for diesel fuel, was performed in a continuous packed bed reactor, at temperatures between 750 and 850°C, at steam to carbon ratios (S/C) between 3 and 6, and in the presence and absence of sulfur (introduced as thiophene). Catalyst performance was evaluated in terms of hydrogen yield and reaction efficiency. Deactivation of the catalyst was evaluated and analyzed in terms of a deactivation rate constant calculated by assuming first-order deactivation.

Reactions were conducted in a continuous flow, packed bed reactor. Separate feeds for n-hexadecane and water were introduced into the pre-heater, which was maintained at 550°C. Following the pre-heater, the feed streams were mixed and introduced into the reactor, in which the catalyst sample had previously been inserted. Catalyst samples consisted of a 6 inch strip of stainless steel foil coated with the desired catalyst, and used as prepared by Catacel. Product gases were separated into permanent gases and condensables using a condenser operating with house cooling water. The gas stream was sent to a Shimadzu 2010 gas chromatograph equipped with a 1 m Shincarbon ST microbore packed column and a pulse-discharge ionization detector. Liquid samples were collected and analyzed off-line.

An experimental design was established to evaluate the performance of the palladium catalyst under a range of operating conditions. Three variables were to be tested (temperature, S/C, and sulfur loading), leading to an nine point experimental design.

Results and Discussion

Hydrogen yield was based on the stoichiometry of the reaction. Assuming complete conversion of hexadecane to CO2 and water provides:

$$C_{16}H_{34} + 32\,H_2O \rightarrow 16\,CO_2 + 49\,H_2$$

Then, the yield of hydrogen can be evaluated based on the molar flow rate of the feed hexadecane:

$$Yield = \frac{F_{H_2,out}}{49F_{C_{16},in}}$$

First order reaction rate constant and the rate constant for deactivation were calculated from the experimental data using a best-fit regression. Assuming first-order kinetics, and exponential decay, the conversion can be related to the residence time and on-stream time according to

$$-\ln(1-X) = k_0\tau\exp(-k_d t)$$

and thus a plot of ln(-ln(1-X)) vs. t provides a straight line, the slope of which is –kd and the intercept is ln(k_0).

The results from these experiments are provided in Table 1, in terms of maximum yield, deactivation rate constant and first order rate constant obtained for a particular experimental run. In general, first order rate constant was higher at higher temperatures and S/C ratios, but was lower in the presence of sulfur than in its absence. Similarly, deactivation was more rapid in the presence of sulfur, at low S/C ratios, and at lower temperatures. These results are consistent with what is previously known about the performance of steam reforming catalysts.

Since the catalyst was deactivated throughout the course of an experimental run, greater detail is provided in graphical format, in which the H_2 yield is compared as a function of on-stream time. Such results are provided in Figure 1, which illustrates the effect of S/C ratio at several different experimental conditions (T = 850°C, and S = 0, 50 ppm). In all cases, it can be seen that all of the samples deactivated during approximately 20 hr of on-stream time, and that the rate of deactivation was greater for the catalysts run at more difficult conditions (low S/C ratio, low temperature, and high sulfur loading). Samples tested at 850°C and S/C = 6 had the greatest hydrogen yield and the slowest rates of deactivation. Reactions run at the severe conditions (850°C ,50 ppm sulfur and S/C=3) produced very low levels of hydrogen even at short times on stream, demonstrating the rapid deactivation brought on by the presence of sulfur.

The reaction not only became less effective at longer times, but the composition of the gas product also changed. At longer times on stream and thus greater amounts of deactivation, thermal cracking products including ethane and ethane were detected in the gas product, at increasing concentrations. The amount of CO relative to CO_2 also decreased at longer run times.

[*] Corresponding Author. E-mail: martin.abraham@utoledo.edu

Table 1
Summary of Experimental Lab Reactor Results

Temp. (°C)	S/C	Sulfur (ppm)	H_2 Yield	k_0 (hr^{-1})	k_d (hr^{-1})
750	3	0	24.00	1090.9	5.16E-02
850	3	0	40.00	1746.6	5.28E-02
750	6	0	62.00	5878.6	6.00E-03
850	6	0	92.00	9683.1	2.64E-03
750	3	50	21.00	479.1	7.20E-02
850	3	50	28.00	1477.5	6.00E-02
750	6	50	48.00	3970.8	1.44E-02
850	6	50	85.00	9026.7	1.08E-02
800	4.5	25	80.00	4402.5	2.88E-02

A: 850°C, 0 ppm sulfur

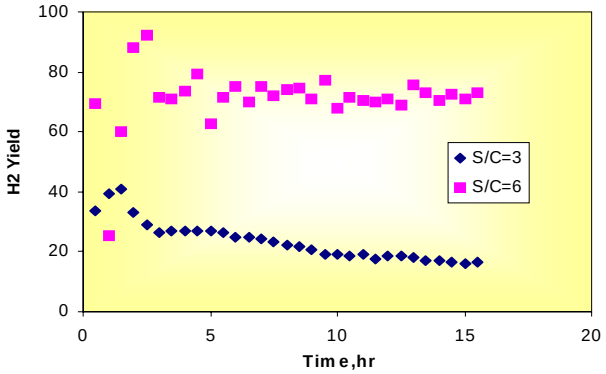

B: 850°C, 50 ppm sulfur

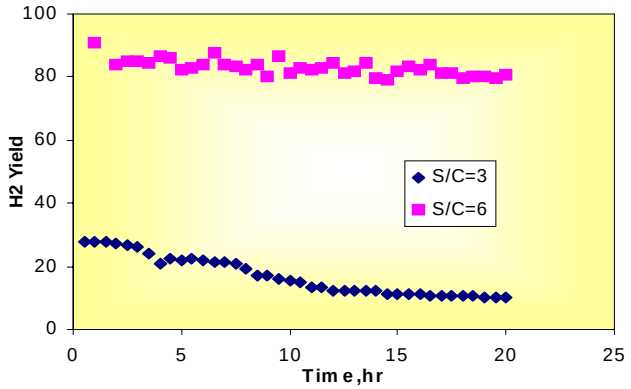

C: Deactivation Plot

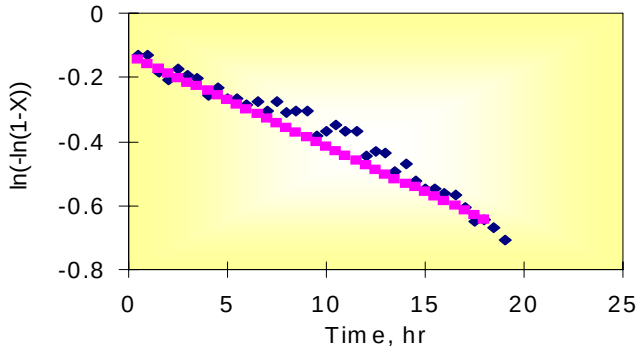

Figure 1. Summary of hydrogen yield at various experimental conditions, and the deactivation of catalysts during time on-stream.

In order to develop a more stable catalyst, the catalyst support matrix was enhanced with the presence of base metal oxides. Both CuO and ZnO were included in the catalyst matrix, at various loadings, and the performance of each of these samples was evaluated under standard reaction conditions of 800°C, S/C = 4.5, and 25 ppm sulfur. The catalyst without any base metals revealed the greatest activity of all samples, but also deactivated fairly rapidly. The samples with 5% CuO and ZnO (at either 2.5% or 5%) had the lowest rates of deactivation. The catalyst containing 5 wt % CuO and 2.5 wt % ZnO appeared to provide the best overall performance, based on a combination of catalytic activity and stability. As was observed with the unmodified catalysts, the composition of the gas product changed as a function of the time on stream, with the presence of cracking products observed at longer times and higher amounts of deactivation.

Analysis is currently ongoing to evaluate the catalyst surface area prior to reaction and compare them with those after the reaction. A more detailed kinetic analysis is also underway, to determine the reaction pathways that are more greatly impacted by the presence of sulfur and catalyst deactivation.

Significance

The conversion of distillate fuels to hydrogen is a critical technology path in the use of fuel cells as auxiliary power units for trucks and jet aircraft. Because of the presence of high sulfur levels in these fuels, the development of sulfur-tolerant reforming catalysts are essential. The current work provides further analysis of the influence of sulfur on the performance of steam reforming catalysts, and demonstrates a new generation of reforming catalysts that provides greater sulfur tolerance. The use of a monolith supported catalyst provides a unique operational advantage in that it permits a reforming device that is more lightweight and compact than existing units, thereby providing a unique opportunity for commercialization.

Acknowledgement.

Financial support for this project was provided by the National Science Foundation through an SBIR grant to Catacel Corp. and by the Ohio Department of Development through the Wright Fuel Cell Group.

References

[i]. Q. Ming, T. Healey, L. Allen, and P. Irving, *Catalysis Today*, **77** (2002) 51.

[ii]. G. Steinfeld *et al.*, AIChE Spring 2000 Meeting, March 5-9, 2000, Atlanta, GA.

[iii]. S. Allen, E. Ashey, D. Gore, J. Woerner and M.C. Cervi, *Naval Engineers Journal*, **110**(1998) 93.

CO_2 REFORMING OF METHANE OVER PLASMA PREPARED Pt/ZrO_2

*Xinli Zhu and Chang-jun Liu**

Key Laboratory for Green Chemical Technology, School of Chemical Engineering and Technology, Tianjin University, Tianjin 300072, China

Introduction

Methane and carbon dioxide are the two major man-made greenhouse gases. CO_2 reforming of methane can convert them into CO and H_2, further to synthesize valuable fuels and chemicals, e.g., ethylene and alcohols. Syngas produced by this reaction has a CO to H_2 ratio of near 1, which is particularly suitable for Fisher-Tropsch synthesis. CO_2 reforming of methane has attracted a worldwide attention. Various transition metals based catalysts have been tested for CO_2 reforming, including Ni, Rh, Pt and Co[1-7]. Although Ni based catalyst has been extensively studied, the problem of deactivation due to coke formation has not well resolved. Pt and Rh based catalysts also attracts much attentions according to their high activity and better performance of anti-carbon. Lercher and his coworker [2, 3, 7] developed a Pt/ZrO_2 catalyst showed better stability for CO_2 reforming. They also argued that Pt atoms on the support-metal perimeter determine the activity. In our previous work, we have successfully loaded Pd[8,9] and Pt[10] on ZSM-5 zeolite with a improved dispersion and quite smaller size of active particles using plasma treatment following calcinations thermally, compared to conventional wetness impregnation method. As a noble metal, it is necessary to reduce the Pt consumption in the catalyst.

In this work, we attempted to prepare more active Pt/ZrO_2 catalyst by the above-mentioned plasma technology. For the purpose of comparison, the catalyst prepared by conventional wetness impregnation was also tested.

Experimental

Catalyst preparations. Zirconium hydroxide was prepared from an aqueous solution of $ZrOCl_2 \cdot 8H_2O$ (Alfa Aesar, > 999%) by hydrolysis with adding NH_4OH aqueous solution up to pH 9.8. After still placed for 12 h, the precipitate was filtered and washed with deionized water till no Cl^- was detected by 0.1 mol/L $AgNO_3$ solution. The gel obtained was dried at 383 K to form $Zr(OH)_4$. Pt was introduced onto the $Zr(OH)_4$ by impregnation with calculated H_2PtCl_6 aqueous solution for 12 h, followed by drying at 383 K for 12 h and calcinations at 923 K for 5 h to obtain conventional Pt/ZrO_2 (denoted as Pt/ZrO_2(C)). To prepare catalyst using plasmas, after dried at 383 K for 12 hrs, $Pt/Zr(OH)_4$ was first treated by argon glow discharge plasma. The obtained sample was then calcined at 923 K for another 5 hrs to obtain the plasma treated Pt/ZrO_2 (denoted as Pt/ZrO_2(P)). The details of plasma treatment have been described elsewhere previously[9,11]. The Pt loading for all the catalysts is 0.5 wt.%.

Catalytic performance. Catalytic performance was tested in a quartz tube with an inner diameter of 4 mm from 823 K to 1073 K increasing by a step of 50 K at ambient pressure. Typically, 50 mg catalyst was packed in the down-flow quartz tube. The catalyst was reduced by high purity hydrogen (> 99999 %) with a flow rate of 20 ml/min at 923 K for 2 hrs before reaction. Then CH_4 and CO_2 (> 99.999 %) with a ratio of 1:1 were introduced into the micro reactor by mass flow controllers at given reaction temperature. At each reaction temperature spot, after stabilized for 20 min, the products sample were collected three times, then the reaction temperature was increased to the next spot. The gas hourly space velocity (GHSV) was 2.4×10^4 ml/(g-cat • h). Products after reaction passed through an ice strap to condense water, and then online analyzed by a gas chromatograph (Agilent 6890) equipped with a thermal conductivity detector (TCD) using a TDX-01 packed column and argon as carrier gas.

Results

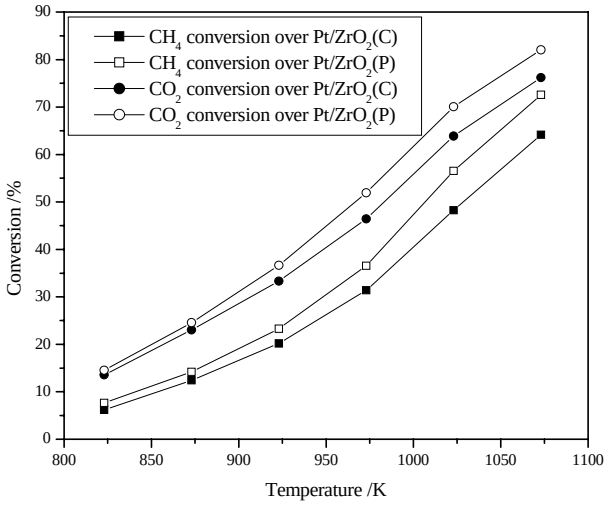

Figure 1. Effect of reaction temperature on conversion of CH_4 and CO_2. Reaction conditions: GHSV=2.4 × 10^4 ml/(g-cat • h), CH_4/CO_2=1:1.

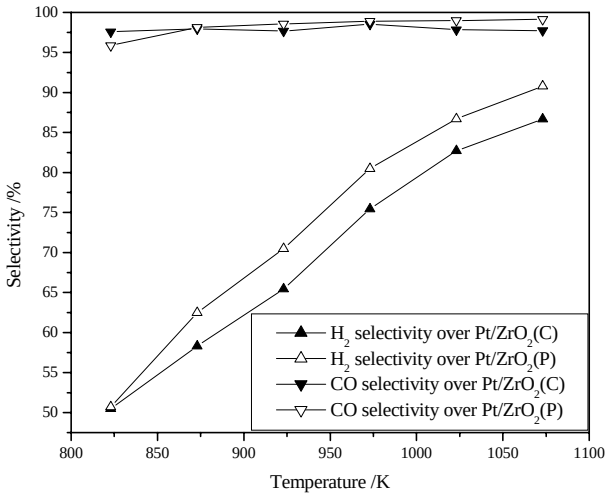

Figure 2. Effect of reaction temperature on selectivity of H_2 and CO. Reaction conditions: GHSV=2.4×10^4 ml/(g-cat • h), CH_4/CO_2=1:1.

The effect of reaction temperature on the conversion of CH_4 and CO_2 is presented in **Figure 1** At the reaction temperature of 823 K, the conversion of CH_4 over Pt/ZrO_2(P) is 1.5 % higher than that over

Pt/ZrO_2(C). With the reaction temperature increasing from 823 K to 1073 K, the difference of the conversion of CH_4 over the two catalysts becomes obvious. When temperature increased to 1023 K and 1073 K, conversion of methane over Pt/ZrO_2(P) increases to 8.3 % and 8.4 % higher than that over Pt/ZrO_2(C), respectively. The activity of CO_2 conversion shows the similar trend. The conversion of CO_2 over Pt/ZrO_2(P) is also increased from 1 % to 6 % higher than that over Pt/ZrO_2(C) with temperature increasing from 823 K to 1073 K.

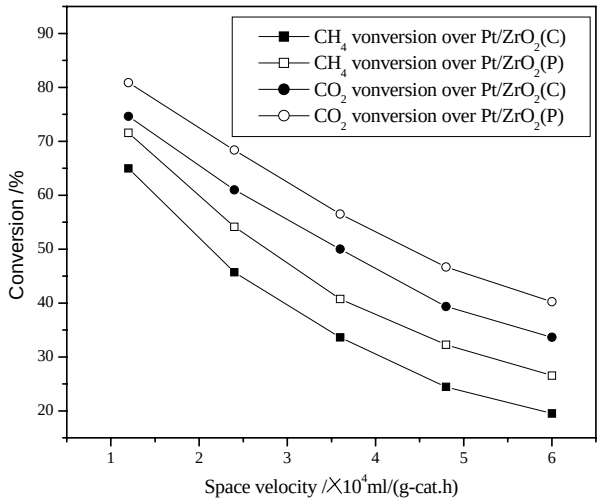

Figure 3. Effect of space velocity on the conversion CH_4 and CO_2. Reaction conditions: Reaction temperature=1023 K, CH_4/CO_2=1:1.

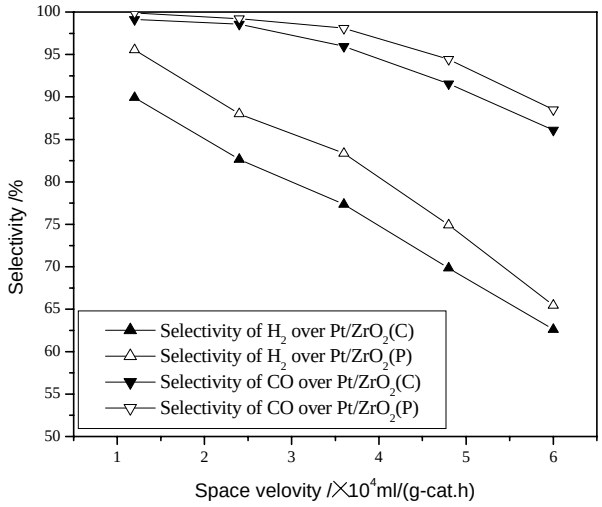

Figure 4. Effect of space velocity on the selectivity of H_2 and CO. Reaction conditions: Reaction temperature=1023 K, CH_4/CO_2=1:1.

Figure 2 shows the effect of reaction temperature on the selectivity of CO and H_2. Both catalysts exhibit high selectivity for CO (more than 95 %), and Pt/ZrO_2(P) possesses a slightly higher of selectivity of CO at most reaction temperatures. The selectivity of H_2 over Pt/ZrO_2(P) illustrates about 4.2 % higher than that over Pt/ZrO_2(C) except reaction temperature at 823 K.

Figure 3 and **Figure 4** demonstrate the effect of space velocity on conversion of CH_4 and CO_2, selectivity of CO and H_2, respectively, at reaction temperature of 1023 K. With the space velocity increasing from 1.2×10^4 ml/(g-cat • h) to 6.0×10^4 ml/(g-cat • h), the conversion of CH_4 and CO_2 decrease near lineally. The conversion of CH_4 and CO_2 over Pt/ZrO_2(P) are 6.0%-8.4% and 6.2%-7.4%, respectively, higher than those over Pt/ZrO_2(C). The selectivity of CO and H_2 are also decreased with space velocity increasing over both the two catalysts, but them over Pt/ZrO_2(P) are 0.8%-2.8% and 2.8%-5.5% higher than those over Pt/ZrO_2(C).

Conclusion

Pt/ZrO_2 catalyst was prepared using plasma treatment following by calcinations thermally. Its activity was compared to the catalyst prepared conventionally. Higher conversion and better selectivity present over the plasma prepared catalyst. Moreover, the activity and selectivity of plasma prepared Ni/Al_2O_3 catalyst even exhibit a more significant improvement, which will be reported later.

Acknowledgment. The support from National Natural Science Foundation of China is very appreciated (under the contract 20225618).

References

(1) Ashcroft, A. T.; Cheetham, A. L.; Green, M. L.; Vernon, P. D. F. *Nature*, 1991, *225*, 352.
(2) Bitter, J. H.; Seshan, K.; Lercher, J. A. *J. Catal.*, 1997, *171*, 279.
(3) Bitter, J. H.; Seshan, K.; Lercher, J. A. *J. Catal.*, 1998, *176*, 93.
(4) Bradford, M. C. J.; Vannice, M. A. *Appl. Catal. A*, 1996, *142*, 73.
(5) Ding, R. G.; Yan, Z. F. *Catal. Today*, 2001, *68*, 135.
(6) Wang, S. B.; Lu, G. Q. M. *Appl. Catal. B*, 1998, *16*, 269.
(7) Bitter, J. H.; Hally, W.; Seshan, K.; Ommen, J. G. V.; Lercher, J. A. *Catal. Today*, 1996, *29*, 349.
(8) Liu, C.-J.; Yu, K.-L.; Zhang, Y.-P.; Zhu, X.-L.; He, F.; Eliasson, B. *Catal. Commun.*, 2004, *4*, 303.
(9) Liu, C.-J.; Yu, K.-L.; Zhang, Y.-P.; Zhu, X.-L.; He, F.; Eliasson, B. *Appl. Catal. B*, 2004, *47*, 95.
(10) Zhang, Y.-P.; Ma, P.-S.; Zhu, X.-L.; Liu C.-J.; Shen, Y.-T.; *Catal. Commun.* 2004, *5*, 35.
(11) Liu, C.-J.; Vissokov, G.P.; Jang, B. W. L. *Catal. Today*, 2002, ***72***, 173.

HYDROGEN PRODUCTION: AN OVERVIEW

David L. King

Energy Science and Technology Directorate
Pacific Northwest National Laboratory
P.O. Box 999, Richland, WA 99354
Fax: 509-375-2186, david.king@pnl.gov

Overview

Hydrogen is an attractive energy carrier because it can be produced from many sources, is a clean burning fuel that does not contribute to greenhouse gas emissions, and has the potential to significantly reduce the U.S. dependency on foreign oil. In the short term, it is anticipated that hydrogen will be produced from fossil fuels via reforming, an approach that still will co-produce CO_2. Thus, hydrogen production and consumption as a whole will still contribute to greenhouse gas production. This initial phase will also be necessary in order to establish the infrastructure for a hydrogen economy, define codes and standards, deal with safety issues, and gain public acceptance for the technology. In the longer term, the vision is to move hydrogen production to renewable sources based on biomass or solar energy, or through other sources that do not emit greenhouse gases, such as nuclear power. Coal may also be an important long term source of hydrogen, but carbon sequestration will be necessary to avoid greenhouse gas production. Thus, each approach to hydrogen production has its own benefits and challenges as well as the scale at which it is most efficient. This presentation will describe some of the technological approaches that are currently being examined for the production of hydrogen for both the short and long term, with an emphasis on the status of the technology, recent advances, and the challenges that remain.

PRESSURE SWING REFORMING OF LIQUID FUELS FOR HYDROGEN PRODUCTION

R. F. Socha, P. J. Berlowitz, F. Hershkowitz

ExxonMobil Research and Engineering Company
P.O. Box 998 Annandale, NJ 08801

Introduction

Steam reforming of hydrocarbons is a widely used process for manufacturing hydrogen on an industrial scale. Coupling this process, or other processes like partial oxidation and autothermal reforming, with a fuel cell presents significant challenges. Energy efficiency is a major design consideration, and at the scale of most fuel-cell applications, this along with rapid start-up and dynamic performance requirements dictate the characteristics of the system.

Pressure Swing Reforming (PSR) is a new process for the production of hydrogen from hydrocarbon fuels. It was first demonstrated in our laboratories using methane as the fuel. We have now extended the operation to a variety of gasoline-range fuels having sulfur contents up to 320 ppm. PSR uses a cyclic reverse-flow reactor to generate high-pressure (e.g., about 1000 kPa) undiluted synthesis gas ($CO+H_2$) at high temperature (up to about 1200°C) over a reforming catalyst, while the inlet and outlet gases remain at a relatively low temperature (less than 400°C). First, the reactor packing is heated by performing a regeneration step, burning waste fuel and air at low pressure as shown in the top of Figure 1. The process flow is then reversed with the primary fuel (e.g., gasoline) and steam as reactants and syngas as the product. This reaction can be run at higher pressure, especially if the fuel and water are initially present in the liquid phase and pressurized. The total cycle time (reforming plus regeneration) can be varied over a range of 5 seconds to 5 minutes in response to the overall flow rate.

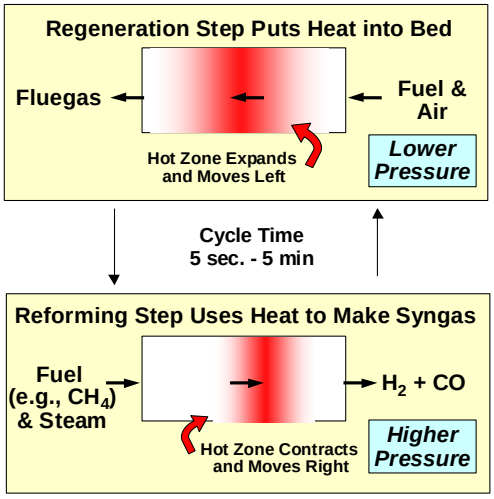

Figure 1. Cyclic reactor system moves heat in time - not across metal walls

The PSR minimizes the need for external heat exchange, making the process highly compact and efficient, and ideally suited to small systems incorporating a fuel cell.

To produce pure H_2, the synthesis gas is then fed to a separation step, which could be based on a membrane or pressure-swing adsorption. The purified hydrogen is then passed to a fuel cell, while the waste fuel returns to the PSR and is used to heat the catalyst. The O_2-depleted air from the fuel cell cathode is used as the oxidant. This configuration is shown schematically in Figure 2.

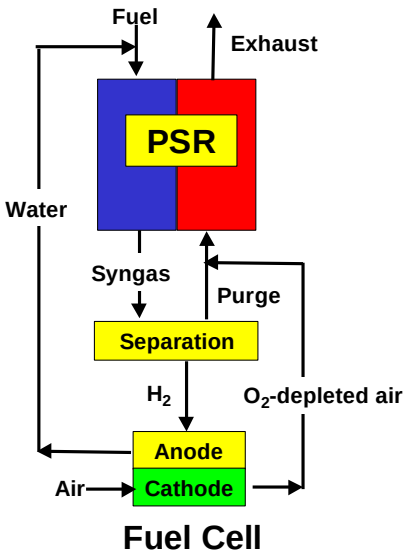

Figure 2. Simplified schematic of PSR integration with a fuel cell

Experimental

Reactions are carried out in the stainless steel double reactor shown in Figure 3. The gasoline fuel is injected into flowing steam in a specially designed mixer and fed to one or the other of the reactors though air-operated valves. While reforming is proceeding in one reactor, hydrogen (as a convenient surrogate for waste fuel) is combusted in the other reactor to provide the needed heat. The inlets and outlets to the two reactors are then switched so that reforming takes place in the second while the first reactor is reheated. The products are analyzed using an on-line mass spectrometer and samples are taken for quantitative analysis by gas chromatography.

The catalyst is a noble-metal washcoated on ceramic honeycomb monoliths. The total internal volume is about 1 liter. The entire operation is automated using LabVIEW software.

Figure 3. Dual-reactor for Pressure Swing Reforming (PSR)

Results and Discussion

We have been able to achieve gasoline conversions of greater than 95% at a gas hourly space velocity (GHSV) of 2500 (based on moles of carbon in the feed, equivalent to a space velocity of ~25,000 for typical catalytic partial oxidation or " autothermal" reformers) for many hours of operation. The conversion depends on a number of factors including the GHSV, the temperature and pressure in the reforming zone, the length of the operating cycle and the sulfur content of the gasoline feed.

Conclusions

ExxonMobil has demonstrated a novel process for the production of synthesis gas (and hydrogen) from liquid hydrocarbon fuels. This technology makes use of a cyclic reverse-flow scheme, which is more efficient than other current processors, especially on the scale used to power fuel-cell vehicles. We see numerous potential applications, including distributed hydrogen production, on-board Auxiliary Power Units (APUs), mobile, and automotive power.

Acknowledgement. We thank Bruce DeRites, Jeff Grenda, George Walchuk, John Brody, Greg DeMartin, John Siller, Elise Marucchi-Soos, Jeff Frederick, Rajeev Agnihoutri and Nick Rados for their contributions to this work.

STEAM REFORMING OF ALCOHOLS FOR HYDROGEN PRODUCTION

Yong Wang, Cathy Chin, Robert Dagle, Hyun-Seog Roh, David L. King, Jamie Holloday, and Daniel Palo

Pacific Northwest National Laboratories, 902 Battelle Blvd, Richland, WA 99352,

Introduction

Steam reforming of methanol and ethanol were studied. They both present different challenges. Methanol is clean, easy to activate, and is potentially an excellent fuel for hydrogen production for portable power applications. Conventional CuZnAl catalysts for methanol steam reforming have the disadvantages such as poor thermal stability and pyrophoric nature. We have developed a highly active and stable PdZn based catalysts for methanol steam reforming. Ethanol is renewable feedstock. Reforming of ethanol presents different challenges, particularly in improving hydrogen yield and minimizing catalyst deactivation due to coke formation. A highly active and selective Rh based catalyst has been developed for this particular applications

Results and Discussion

Steam reforming of methanol has been studied as a source of hydrogen production for the fuel cell due to its high hydrogen/carbon ratio, low sulfur content, and relatively low reforming temperature (250-350ºC) [i] Formation of CO as a by-product should be minimized to avoid deterioration of the fuel cell by CO adsorption. Most studies have been focused on Cu based catalysts which exhibit high selectivity to CO_2 and H_2[ii]. Copper based catalysts, however, have the disadvantages of poor thermal stability above 270°C and pyrophoric characteristic. Group VIII metals are markedly different from the copper catalysts. Over Group VIII metals catalysts methanol decomposes to CO and hydrogen. On the other hand, Iwasa *et al* were the first to report that Pd supported on ZnO and reduced at > 300℃ has exceptionally high activity and selectivity to CO_2 and H_2 [iii]. The intriguing and promising performances of Pd/ZnO catalysts were attributed to PdZn alloy formation[iv]. The small amount of CO over PdZn catalysts in all literature reports was attributed to a small amount of metallic Pd species [v] which may be related to the catalyst preparation[vi]. We have confirmed this hypothesis using *in-situ* X-ray absorption experiments on the samples prepared using two different methods.

In the initial stages of our work on ethanol steam reforming, the role of the catalyst support was examined for ethanol steam reforming using Rh as the active metal. Rh was chosen since it is known to exhibit the highest activity of all the precious metals. It was also found that support identity rather than metal dispersion has significant effects on the activity with Rh/CeO_2-ZrO_2 exhibiting the best H_2 yield among the catalysts studied. In a subsequent series of experiments, the CeO_2-ZrO_2 support pre-calcination and catalyst calcination temperatures were systematically varied to evaluate the metal-support interaction and the related effects on H_2 yield. It was found the support pre-calcination temperature is not a significant factor between 500 and 800 ^oC despite the potential for sintering the CeO_2 phase. It has been established that acetaldehyde is a reaction intermediate and easily undergoes decarbonylation to form CH_4 and CO. Once CH_4 forms, high temperatures are required to reform it into CO and H_2. Therefore, in order to maximize H_2 formation, the CH_3 group (which is the precursor to CH_4) needs to be oxidized with steam before CH_4 is allowed to form. It is possible that Ce sites in CeO_2-ZrO_2 are partially oxidized under reforming conditions and these partially oxidized sites provide active oxygen species, which may suppress CH_4 formation. We speculate that the catalyst with appropriate pretreatment has better interaction between Rh and support as a result of the single calcination, resulting in more effective oxygen transfer. Further physicochemical characterization of this catalyst system will be presented.

References

[i] Peters, R.; Dusterwald, H.G.; Hohlein, B. *J.Power Sources*, 2000, 86, 507.
[ii] Trimm, D.; Onsan, Z.I. *Catal.Rev.*, 2001, 43 (1&2), 31.
[iii] Iwasa, N.; Kudo, S.; Takahashi, H.; Masuda, S.; and Takezawa, N. *Catal.Lett.*, 1993, 19, 211.
[iv] Chin, Y.; Dagle, R.A.; Hu, J.; Dohnalkova, A.C.; Wang,Y. *Catal.Today*, 2002, 77, 79.
[v] Suwa, Y.; Ito, S.; Kameoka, S.; Tomishige, K.; and Kunimori, K. *Appl.Catal.A:General*, 2004, 267, 9.
[vi] Chin, Y.; Wang, Y.; Dagle, R.A.; Li, X. *Fuel Processing Tech.*, 2003, 1681, 1

ANALYSES OF HYDROGEN PRODUCTION FROM SUB-QUALITY NATURAL GAS (II): SQNG STEM REFORMING AND AUTOTHERMAL STEM REFORMING

Cunping Huang, and Ali T-Raissi
Florida Solar Energy Center
University of Central Florida
1679 Clearlake Road
Cocoa, FL 32922

Introduction

Part (I) of this paper [1] has analyzed sub-quality natural gas (SQNG) pyrolysis and autothermal pyrolysis. Production of hydrogen via direct thermolysis of SQNGs produces two moles of hydrogen instead of four achieved by the steam reformation process. The main advantage of methane pyrolysis is the elimination of carbon dioxide production. However, coke formation that can cause catalyst deactivation occurs during the thermal decomposition of methane. Although some carbon-based catalysts may be able to resist deactivation, the lifetime of the catalysts still remains a big challenge.

The objective of Part (II) of this paper is to further explore the applicability of conventional technologies, namely steam reforming of methane (SRM) and autothermal steam reformation, in the treatment of SQNGs. Similarly to Part (I), a Gibbs reaction unit operation in the AspenPlus^{TM} chemical process simulator was applied as a thermodynamic analytic tool for equilibrium calculations for the SQNG + H_2O and SQNG + H_2O + O_2 systems. The main focus of the paper is to investigate the stability of hydrogen sulfide in these processes.

Steam reforming of SQNG (SRSQNG)

The compositions of SQNG applied in this paper are the same as in Part (I) with a 10% hydrogen sulfide concentration. The total carbon is calculated from the total hydrocarbons in SQNG, which is 110.10 mol/hr. The thermodynamic analyses are conducted in isothermal conditions, assuming that the inlet component mole flow rates are equal to their mole fractions. The inlet water flow rates are calculated based on the ratio of water to the total carbon moles (110.10 mol/hr), x = H_2O/C. The ratio of x is selected as: 0.25, 0.50, 0.75, 1.0, 1.5 and 2.0 corresponding the mole flow rates of 27.25, 55.05, 82.575, 110.10, 165.15 and 220.20 mol/hr, respectively.

Equilibrium flow rates of CH_4, H_2 and C. **Figure 1** demonstrates the flow rate of CH_4, H_2 and C with the reforming temperatures. CH_4 decomposition during SRSQNG is similar to that in SQNG pyrolysis. At temperatures above 850 ^oC since all the hydrocarbons are consumed, the hydrogen outlet rate remains constant. Compared to SQNG decomposition, which produces a maximum of 200kmol/hr hydrogen, the hydrogen production rate during the course of SRSQNG increases with water inlet flowrate and is greater than 200 kmol/hr. The greater hydrogen production results from the water splitting. However, when x is greater than 1.0, no significant increase in hydrogen production can be observed. When x = 2.0, the maximum hydrogen output is about 300 kmol/hr, indicating that only 100 kmol/hr of hydrogen is from the splitting of water, representing about 50% of the total water inlet. Water conversion increases with the decrease of water input, and reaches 100% when x is less than 1.0, suggesting that one mole of carbon can only split one mole of water in SRSQNG for the production of hydrogen.

In order to preclude carbon coke production during SRSQNG, the ratio x must be controlled. Carbon flow rates decrease with the increase of water inlet flow rate. At a lower x (< 1.0), carbon lay down occurs throughout the entire temperature range. Only when x > 1.0 does the carbon flow rate decrease to zero when the temperature is greater than 900 ^oC. This criterion is important to the reforming process in order to prevent catalyst deactivation.

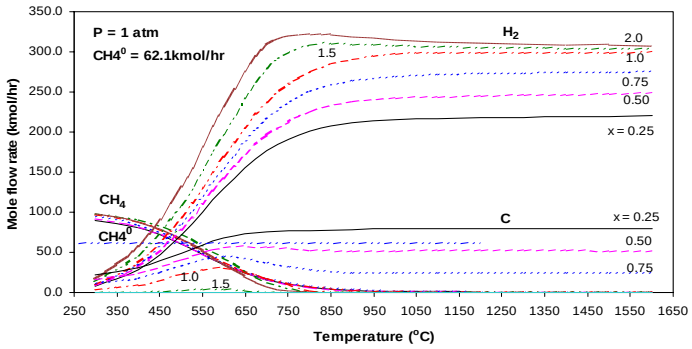

Figure 1. Equilibrium flow rates of CH_4, H_2 and C in SRSQNG (x = 0.25 to 2.0)

Equilibrium flow rates of H_2S, CS_2 and S_2. The equilibrium flow rates of H_2S at different x ratios are illustrated in **Figure 2**. The initial mole fraction of H_2S is 10.0%, corresponding to 10.0 kmol/hr inlet to a Gibbs reactor. H_2S decomposition during SRSQNG is similar to that in SQNG pyrolysis. H_2S does not significantly decompose at different water input levels when temperature is lower than 1200 ^oC, indicating that it is stable and can be considered as an inert gas in these conditions. Even when temperature is as high as 1600 ^oC, H_2S decomposition increase is still less than 30%. Interestingly, at temperatures greater than 1200 ^oC, water influence on the H_2S conversion can be separated into two significant ranges: when x < 1.0, H_2S conversion is higher than that when x > 1.0, suggesting that higher water input favors the stability of hydrogen sulfide.

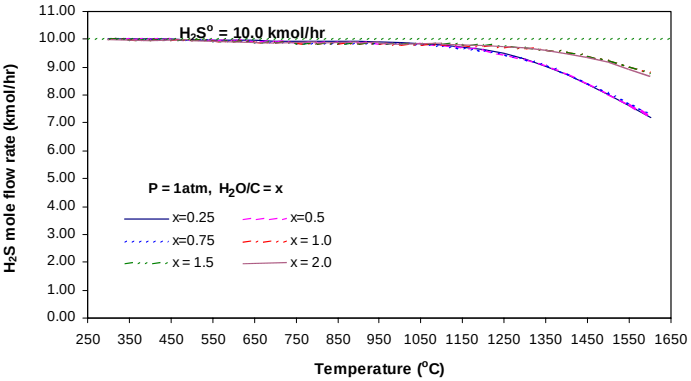

Figure 2. Equilibrium flow rates of H_2S in SQNGSR (x = 0.25 – 2.0)

Figure 3 illustrates the equilibrium flow rates of COS, CS_2 and S_2, which are dependent upon both temperature and input water flow rates. No SO_2 (or SO_3) is generated in the equilibrium mixture, showing that SRSQNG does not produce sulfuric acid gas, and therefore no environmental impact exists. Since SRSQNG occurs at temperatures between 700 to 900 ^oC, even though COS is a major byproduct its concentration is at a ppm range. The formation of COS is similar to the water gas shift process based on the reaction: CO + H_2S = 0.5H_2 + COS. Additionally, small amounts of CS_2 can be

observed when temperature exceeds 1200 °C. **Figure 4** indicates that the maximum CS_2 output flow rate occurs at a temperature of 1600 °C and is about 1.0 kmol/hr, accounting for less than 0.4% of total output gases. CS_2 is produced according to hydrogen sulfide methane reformation: $CH_4 + H_2S = 4H_2 + CS_2$.

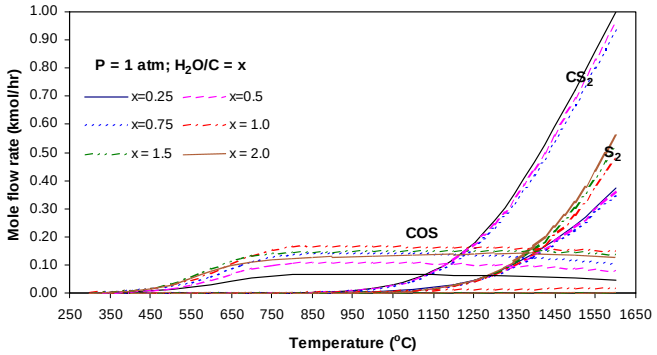

Figure 3. Equilibrium flow rates of COS, CS_2 and S_2 in SRSQNG (x = 0.25 – 2.0)

Autothermal steam reformation of SQNG (Auto SRSQNG)

SRSQNG is a highly endothermic process, requiring a large amount of energy input. To reduce the dependence of external energy sources, we can burn part of hydrocarbons in SQNG and the heat produced by internally burning can provide energy for SRSQNG. Two systems, SQNG + $0.0625H_2O$ + yO_2 and SQNG + $0.25H_2O$ + yO_2 are selected for investigating oxygen effects on SQNGSR. This preprint shows only results of x = 0.25.

Equilibrium flow rates of CH_4 and H_2. **Figure 4** depicts equilibrium flow rates of CH_4 and H_2 at various inlet oxygen levels, with x=0.25. Similar to the SQNG pyrolysis, all other hydrocarbons are decomposed into H_2, CH_4 and C within a temperature range of 300 ºC to 500 ºC. The CH_4 flow rates decreases with increases of either temperature or oxygen flow rate. On the other hand however, H_2 flow rates are independent of oxygen input ratio at y less than 0.375. When y increases to 0.50, hydrogen flow rate slightly decreases. The decrease is more significant for x=0.25 than for x=0.0625.

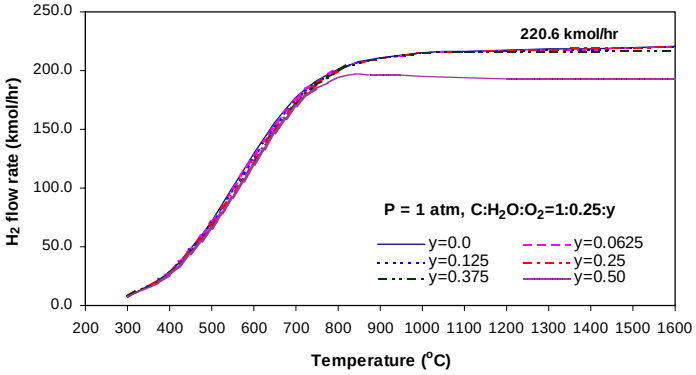

Figure 4. Equilibrium flow rates of CH_4 and H_2 at different oxygen inputs ($C:H_2O:O_2$=1:0.25:y)

Equilibrium mole flow rates of H_2S, COS, CS_2 and S_2. Equilibrium outputs of H_2S at x = 0.0625 and 0.25, with varying levels of oxygen input are similar to **Figure 2,** indicating the stability of H_2S during the course of autothermal SRSQNG. Unlike the effect of water on COS output rates, increasing the oxygen inlet rate results in the higher COS production rates shown in **Figure 5.** The effect is more significant at a low water input level. However, the effects of O_2 on output rates of CS_2 and S_2 are similar to the effects of H_2O.

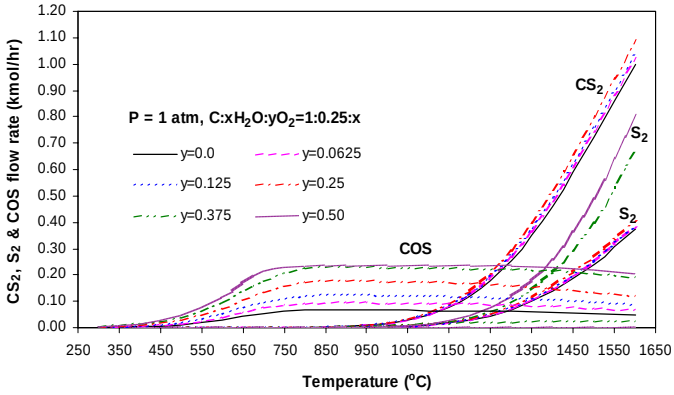

Figure 5. Equilibrium flow rates of COS, CS_2 and S_2 at different oxygen inputs ($C:H_2O:O_2$=1:0.25:y)

Heat of the autothermal SRSQNG. Heat requirements for the autothermal SQNGSR are depicted **Figure 6**. With increases in the oxygen inlet flow rate the total heat energy requirement decreases significantly, approaching energy neutral conditions. Comparing water inlet levels (y = 0.0625 and 0.25), it is found that at a higher water input to the system, higher oxygen inputs are required to reach a zero energy requirement condition.

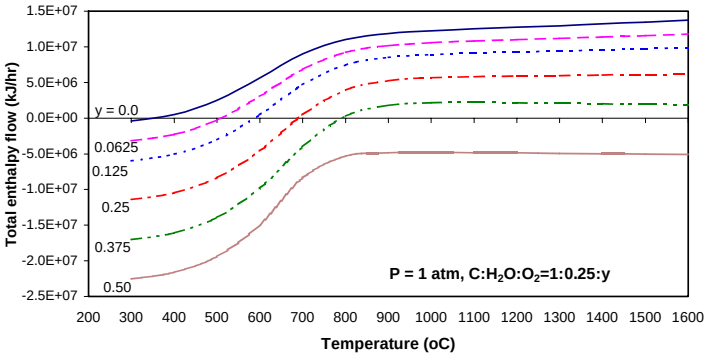

Figure 6. Total enthalpy change at different oxygen inputs ($C:H_2O:O_2$=1:0.25:y)

Acknowledgment

The authors are grateful for the financial support of the NASA-GRC Grant NAG3-2751 hydrogen project.

References

1. Huang, C., and Raissi, A., " Analyses of Hydrogen Production from Sub-quality Natural Gas (I): SQNG thermal decomposition and autothermal process" Preprint of the 230th ACS National Meeting, Washington, Aug 28-Sept 1, (2005)
2. Huang, C., and Raissi, A., " Liquid Hydrogen Production via Hydrogen Sulfide Methane Reformation" Preprint of the 228th ACS National Meeting, Philadelphia, August, 22-26 (2004)

A NEW PROCESS FOR THE PRODUCTION OF HYDROGEN FROM HYDROGEN SULFIDE

Prof.Israel E. Wachs, Andrew G. Gibson

Lehigh University Gibson Technologies
111 Research Drive 2293 LittlebrookeTrace
Bethlehem, PA 18015 Atlanta, GA 30338

Introduction

A new process for the production of hydrogen from hydrogen sulfide is described wherein carbon monoxide is reacted with hydrogen sulfide to produce hydrogen and carbonyl sulfide. The carbonyl sulfide is then reacted with oxygen to produce carbon monoxide and sulfur dioxide. The carbon monoxide is recycled back to the hydrogen sulfide reaction step.

Previous investigators have explored this basic chemistry but conversion and selectivities of desired products have been low. Recently, investigators under Prof. Israel Wachs at Lehigh University, have discovered a class of catalysts that dramatically improve conversion and selectivities to the point where the economics of this technology are a cost effective method of producing hydrogen.

Carbonyl sulfide (COS) is found in many industrial process streams such as those associated with natural gas production, petroleum refineries and coal gasification plants. COS is often catalytically converted by hydrogenation to methane (CH_4), hydrogen sulfide (H_2S), and water; by hydrolysis to carbon dioxide (CO_2) and H_2S, or by oxidation to CO_2 and SO_2. Hydrogenation is an expensive waste of increasingly valuable hydrogen (H_2) while hydrolysis and total oxidation produces CO_2, considered by many to be an environmental threat due to its alleged impact on global warming.

H_2S is encountered in refineries where hydrodesulfurization is widely used to remove sulfur from gasoline. Also natural gas geologic formations may contain as much as 10-30% . The H_2S is typically separated from the methane and the latter is distributed for consumer and industrial use. The H_2S is usually converted to elemental sulfur via the Claus process. In the Claus process, a first portion of the separated H_2S is oxidized by combustion to SO_2 and water. The remaining portion of the H_2S is reacted with water-laden sulfur dioxide in the presence of a suitable catalyst to produce additional water and elemental sulfur. Thus all of the potentially valuable hydrogen is lost to the atmosphere as water (The elemental sulfur is sold as a low priced commodity product).

The Wachs process (patented) would significantly improve the economies of sour gas recovery and would greatly benefit the operation of petroleum refinery operations.

Experimental

A series of experiments using selected metal oxides supported on oxides of different metals resulted in the choice of V_2O_5 on various metal oxides as a family of most effective catalysts for the oxidation of COS and CS_2 to CO and SO_2.

The CO thus generated could then be coupled with the known equilibrium reaction to reduce H_2S with CO , thus producing valuable H_2 and relatively " dry" SO_2.

1) $2COS + O_2 \rightarrow 2CO + SO_2$

2) $2CS_2 + 5\,O_2 \rightarrow 2\,CO + 4\,SO_2$

3) $CO + H_2S \Leftrightarrow H_2 + COS$

The oxidation reaction ,1), is very efficient over catalysts comprising a monolayer of vanadium(V_2O_5) on various metal oxide supports. For the supports examined, the Turnover Frequency trend (TOF) is: $CeO_2 > ZrO_2 > TiO_2 > NbO_2 > Al_2O_3 \sim SiO_2$.

COS and CS_2 are selectively oxidized to CO at yields between 90-100% (Table 1) .

The " dry" SO_2 thus produced (due to the H_2 being formed instead of H_2O) is advantageous to a Claus reactor because it favorably shifts the reaction towards the desired elemental sulfur product. Alternately, if used as a feed to a sulfuric acid plant, the moisture load and impurities to the SO_2 driers are greatly reduced, particularly in comparison to feedstocks obtained from smelters and other industrial sources.

Table 1. Oxidation of COS and CS_2 to CO Over V_2O_5 Supported Catalyst

Reactant	Temperature °C	TOF Yield $10^{-1} \times s^{-1}$	%
COS	330 max	0.3-2.0	90-100
CS_2	270 max	0.2-1.6	90

The CO thus produced is used to reduce the H_2S waste stream to hydrogen and co-product COS (equation (3 above). This COS is recycled to the process along with unreacted COS.

Results

The foregoing chemistry can be used to to design a process that yields valuable hydrogen from H_2S streams which now have only the value of their sulfur content. The hydrogen thus represents a value-added factor to H_2S streams.

In reference (1) a process outline describes the major steps as narrated below. See Figures 1 and 2.

CO may be obtained by oxidizing COS and/or CS_2 from industrial streams or by the steam reforming of methane. Figure 1 illustrates a COS/CS_2 oxidation reactor which may operate at temperatures ranging from 220º C to 350º C and a pressure from atmospheric to 500 psig. The reactants are fed in the vapor phase and contacted with a supported vanadium catalyst. The catalyst may be in the form of pellets or rings in a fixed bed or powder in a fluidized bed. Contact time in a fixed bed wherein the catalyst pellets or rings are packed into the tubes of a shell-and-tube reactor is in the order of 2-10 seconds. The effluent from this reactor contains the desired CO as well as unreacted COS/CS_2, O2, and byproduct SO_2. The components are separated in unit operations known to those skilled in the art. This oxidation reactor is shown again in Figure 2 where an additional fresh stream of COS and or CS_2 may also be introduced

In Figure 2, the hydrogen is generated by reacting H_2S and CO utilizing the known vapor phase equilibrium reaction described by Fukada, et. al., (2) (3). Temperatures in the range of 250ºC to 400ºC and pressures from atmospheric to 500 psig. are employed. A downstream series of separations is required to separate unreacted H_2S and CO for recycle. The H_2S can, for example, be absorbed in amine solutions and thermally desorbed for recycle. Other processing steps can be used to separate the hydrogen from COS.

The hydrogen product is collected and utilized for hydrogenation purposes or as a reactant in hydrodesulfurization

operations in a refinery. The COS is recycled to the oxidation reactor (Fig 1) to regenerate CO for the hydrogen reactor.

The SO_2 from these operations is a desirable feedstock for a sulfuric acid plant or a Claus plant (producing elemental sulfur) because of its low moisture content. The efficiency of both of these operations is enhanced by low moisture.

Conclusions

A catalytic process has been invented which permits the coupling of the known equilibrium reaction to produce hydrogen and a by-product COS with a new oxidation process for utilization of the COS. This is accomplished by oxidizing COS over supported vanadium catalyst(s) which results in high yields of CO. The COS becomes a useful recycle component, being alternately oxidized (by O_2)and reduced by the H_2S, thus yielding valuable hydrogen.

References

(1) Wachs, Israel E., US Patent 6,497,855, *Process for the Production of Hydrogen from Hydrogen Sulfide*, December 24, 2002

(2) Fukada, et. al., *Journal of Catalysis*, 49 3 79 (1977)

(3) Fukada, et. al., *Bulletin of Chemistry for Japan*, 51, 150 (1978)

CONVERSION OF HYDROGEN SULFIDE INTO HYDROGEN AND SULFUR

E. Krisanti, J.J. Robertson, G.B. Lucas, M.A. Plummer, and S.W. Cowley*

Department of Chemistry and Geochemistry
Colorado School of Mines
Golden, CO 90401

*MPr&d
Centennial, CO 80122-3708

Introduction

Hydrogen sulfide removal from natural gas or from gases produced by the petroleum industry typically involves air oxidation of hydrogen sulfide into elemental sulfur and water, as shown in equation (1). The Claus process, a gas phase oxidation reaction, and the Stretford™ process, a liquid phase oxidation reaction, are commonly used to remove hydrogen sulfide and produce sulfur in good quantity[1-2]. The Hysulf℠ process converts hydrogen sulfide directly into valuable hydrogen and sulfur, see equation (2).

$$8H_2S + 4O_2 \rightarrow 8H_2O + S_8 \quad \text{(Claus \& Stretford}^{TM}\text{)} \qquad (1)$$

$$8H_2S \rightarrow 8H_2 + S_8 \quad \text{(Hysulf}^{SM}\text{)} \qquad (2)$$

The Hysulf℠ process has two stages, see figure 1. In the first stage, at a reaction temperature of about 57 °C, hydrogen sulfide reacts with an anthraquinone to make the corresponding hydroanthraquinone and solid sulfur. In the second stage, at a temperature of about 200 °C, the hydroquinone is catalytically dehydrogenated to regenerate the anthraquinone and to make hydrogen gas, where R represents t-butyl in most of this work. Therefore, 2-t-butylanthraquinone is abbreviated as TBAQ and the corresponding hydro-2-t-butylanthraquinone as H_2TBAQ.

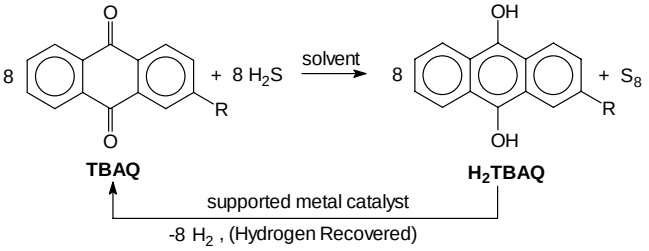

Figure 1. Two stage chemical process for converting H_2S into H_2 and S_8.

Although the Hysulf℠ process looks promising, a better understanding of the fundamental chemistry is required if the process is to be commercialized[3]. It is thought that the formation of a diradical anthraquinone intermediate is necessary for the reaction to proceed. The role of the solvent and substituents groups (R) in forming this diradial intermediate needs to be better defined. The goal of this study is to improve the rate of the anthraquione reduction and sulfur formation reaction in the first stage of the process by gaining a better understanding of the reaction mechanism, including the role of the solvent in promoting this reaction.

Experimental Methods

Reactor Tests. The reduction of TBAQ by H_2S was conducted in either a batch low pressure mini or batch high pressure micro glass stirred-tank reactor. The high pressure mini glass reactor is shown in figure 2. In a typical run, 30-60 mL of solvent containing 15 wt% of 2-t-butylanthraquinone (TBAQ) placed into the

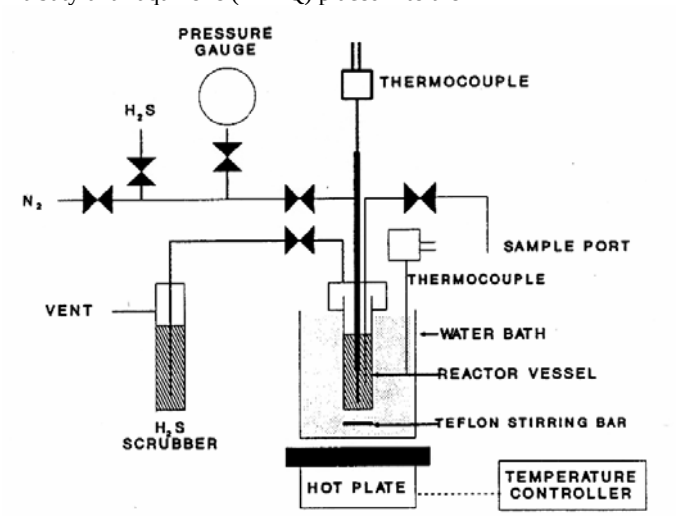

Figure 2. Schematic of batch mini reactor system.

reactor. The micro reactor was purged with N_2 gas for 15 minutes prior to continually flowing 60 cc/min of H_2S through the solution for the micro reactor at atmospheric pressure. Air removal is necessary to prevent oxidation of the H_2TBAQ product. The high pressure micro reactor was purged with N_2 gas prior to charging the reactor at a constant pressure of H_2S. The reaction was continually stirred using a magnetic stirring bar. A water bath was used to control the reaction temperature and an internal thermocouple was used to monitor the reaction temperature. A 1/16 inch o.d. stainless steel siphon tube was used to collect samples for NMR analysis. Unused H_2S was passed through a 1.0 M sodium hydroxide gas scrubber.

Analytical Methods. The effect of solvents and R groups on the formation of the diradical he products of the reaction were observed using a 60 MHz Varian EM360 or a 400 MHz ChemMagnetics NMR. The rate of TBAQ reduction by H_2S was monitored by measuring the increase in aromatic H_2TBAQ hydrogen signals centered at 7.5 and 8.6 ppm. The ratio of the H_2TBAQ peak areas to the total aromatic peak area was used to calculate the mole percent of TBAQ converted to H_2TBAQ.

Details of the TBAQ to H_2TBAQ reaction mechanism were studied using cyclic voltammetry (CV) and an electrochemical cell. A mercaptan or a bisulfide salt was added into the electrolytic cell to replace hydrogen sulfide as the protic agent. Lastly, sodium sulfide salt (NaSH) was added to the TBAQ solution to investigate the effect of the HS^- anion as an electron donor agent.

Results and Discussion

NMR was used to analyze the effect of H_2S pressure, temperature, and solvent polarity on the TBAQ reaction kinetics, and to identify the reaction intermediates produced in the stirred tank reactors. Figure 3 shows the change in the NMR spectrum TBAQ in N,N-dimethylacetamide (DMAC) solvent before and after reaction with H_2S. The reaction rate was found to be first order in H_2S and TBAQ and the rate law is given in equation (3).

$$\text{Rate} = k[H_2S][\text{TBAQ}] \qquad (3)$$

When the H_2S concentration was maintained constant through out the test, the rate is dependant only on the TBAQ concentration and a plot typical of a first order reaction was obtained, see figure 4. Significant TBAQ conversion was first observed after 15-20 minutes, indicating an induction period for the reaction. A

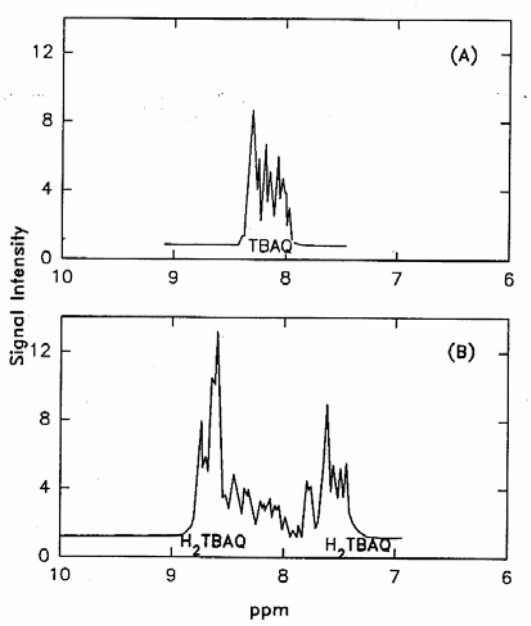

Figure 3. NMR of reactant TBAQ (A) and product H_2TBAQ.

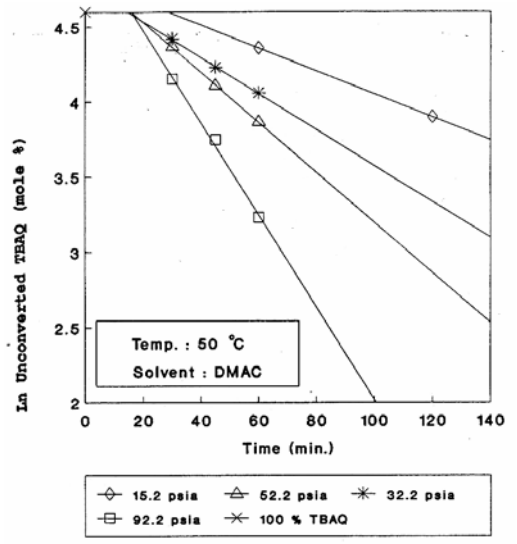

Figure 4. TBAQ conversion as a function of H_2S pressure.

temperature increase of 3 °C was observed when the solution containing TBAQ was initially charged with H_2S. After 2-3 minutes the excess heat dissipated and the reaction returned the desired temperature. The yellow colored feedstock briefly turned a bluish color, which is indicative of a rapid electron transfer reaction. The reaction proceeded to turn a green color and then a reddish brown color, which is indicative of H_2TBAQ formation. Eventually the reaction turned a very dark black color, which is typical of sulfur polymer formation, and finally a yellow solid (sulfur) was observed to precipitate out of solutions. The choice of solvent was also found to have a significant influence on the reaction kinetics. The reaction rate constant for DMAC is larger than that observed for N-methyl-2-pyrrolidinone (NMP). It is reported that H_2S solubility in both solvents is not much different[5-6]. Hence, there is a possibility that the molecular structure of the solvent plays an important role promoting the reaction.

After four hours of reaction time, NMP solvent gave ~53%, DMAC ~70%, N-methylacetamide ~35%, tetrahydrofuran 0%, and γ-butyrolactone 0% conversion of TBAQ to H_2TBAQ. The effect of solvent properties on TBAQ conversion was investigated further by NMR, see figure 5. There is a dramatic change in the NMR pattern

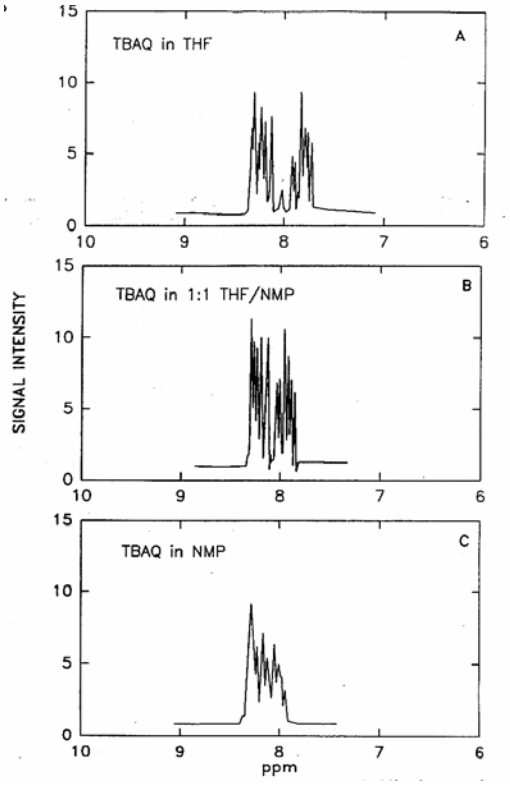

Figure 5. Effect of solvent on the NMR Proton Spectrum of the TBAQ aromatic region.

for the aromatic region of TBAQ as the relatively non-polar solvent THF (μ_D = 1.75 Debye) is replaced by the more polar solvent NMP (μ_D = 4.09 Debye). The NMR data suggest that anthraquinone is converted from the carbonyl to a diradical form as shown in figure 5. Computational analysis and reaction data suggests that the intitial step of the reaction requires the anthraquinone diradical and the formation of an HS^- species. The formation of these species is necessary to provide a good match between the TBAQ LUMO and HS^- HOMO energy levels. Cyclic voltammetry, computational analysis, and NMR analysis were used to obtain a more detailed picture of the reaction mechanism.

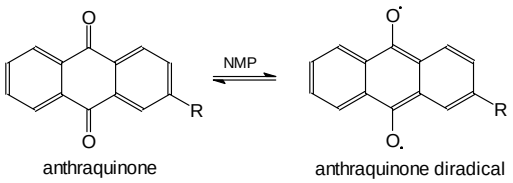

Figure 6. Conversion of anthraquione into anthraquione diradical in NMP solvent.

Conclusions

The experimental data show that solvent polarity is not the primary factor that affects the TBAQ conversion. The ability of the solvent to complex with the H_2S and/or the TBAQ to alter their respective HOMO and LUMO energy levels may be a requirement. Tertiary amides, such as NMP or DMAC, appear to be better solvents for TBAQ reduction than secondary amides, cyclic ethers, alcohols, or lactones.

Acknowledgement. This work was funded by Marathon Oil Company, MPr&d, and GRI.

References

(1) Kohl, A.L., and Riesenfeld, F.C., "Gas Purification, 4th Edition", **1985**, Gulf Publishing Company.
(2) Gary, J.H and Handwerk, G.E., " Petroleum Refining, **1984**, Marcel Dekker.
(3) Plummer, M.A, ""Gas Processing Developments: Sulfur and Hydrogen from H_2S", **1987**, Hydrocarbon Processing, April, 38, pp 38-40.
(4) Murieta-Buevara, F., and Rodrigquez, A.T., **1984**, "Solubility of Carbon Dioxide, Hydrogen Sulfide, and Methane in Pure and Mixed Solvents", J. Chem. Eng. Data, 29, 456.
(5) Hayduk, W. and Pahlevanzadeh, H., "The Solubility of Sulfur Dioxide and Hydrogen Sulfide in Associating Solvents", **1987**, Can. Chem. Eng., 65, 299.

HYDROGEN PRODUCTION AT THE PACIFIC NORTHWEST NATIONAL LABORATORY

Jamie Holladay, Daniel Palo, Robert Dagle, and Yong Wang

Pacific Northwest National Laboratory, 902 Battelle Blvd, MS k6-24, Richland, WA 99352, Fax: 509-376-3108, jamie.holladay@pnl.gov

Overview

Battelle, Pacific Northwest Division (Battelle) is actively developing compact portable or transportable fuel processors for hydrogen production to power hybrid fuel cell power systems. These systems are being developed under programs sponsored by the US Military, DOE, and Battelle. A broad range of fuels, such as methanol, ethanol, propane, natural gas, bench mark gasoline, and synthetic JP8, have been successfully reformed. For low power applications, methanol fuel processors were developed at outputs ranging from sub-watt to several hundred watts. For greater than 1 kW applications, fuel steam reforming systems operating on a variety of fuels, including synthetic JP8, have been developed. Each system employs Battelle's proprietary catalysts and patented microchannel architecture. These technologies enable compact hydrogen production systems for hydrogen storage or direct use in fuel cells. These fuel processors achieve over 70% thermal efficiency. Reactor design, catalyst properties and system considerations will be discussed.

SULFUR TOLERANT FUEL PROCESSING CATALYSTS

S.L. Swartz, G.B. Arkenberg, and E.M. Sabolsky

NexTech Materials, Ltd.
404 Enterprise Drive
Lewis Center, OH 43035

Introduction

A major requirement for near term implementation of fuel cell power generation systems is use of our existing hydrocarbon fuel infrastructure. Fuel cells operating on hydrocarbon fuels will have early opportunities for large market applications within a number of sectors, including residential and industrial heat and power systems, auxiliary power units for cars and long-haul trucks, and a wide array of military power systems. Infrastructure fuels (including natural gas, propane, gasoline, diesel and kerosene) are based on hydrocarbon compounds of differing complexity and contain sulfur impurities of varying amounts. In order for use with a fuel cell, the hydrocarbon fuel is first converted into a gas that is compatible with efficient fuel cell operation. This is the purpose of the fuel processing system. In general, the technical difficulty associated with fuel processing increases with carbon number and sulfur content of the hydrocarbon fuel. Today's technology requires bulky sulfur removal beds, which must be changed frequently and can allow slip into the catalyst beds, leading to catalyst deactivation. Therefore, catalysts that resist deactivation by sulfur would add design flexibility to fuel processor system developers.

Several types of fuel processors currently are being developed for fuel cells where hydrocarbon fuels are being targeted for use. These systems vary depending on the fuel cell type, the targeted fuel, and the design philosophy of the developers. The first step in fuel processing is a catalytic (reforming) stage to convert the hydrocarbon fuel to a syngas mixture of hydrogen and carbon monoxide. This is accomplished by reacting the fuel with water (steam reforming), with oxygen (catalytic partial oxidation), or a combination of steam and oxygen (autothermal reforming). After reforming, the fuel can be fed directly to a molten carbonate or solid oxide fuel cell. However, additional fuel clean-up processing steps are required before the fuel can be used within a PEM fuel cell, which require extremely clean hydrogen. These includes the water-gas shift (WGS) reaction to increase hydrogen content and reduce carbon monoxide content ($CO + H_2O \rightarrow CO_2 + H_2$), and selective oxidation ($CO + O_2 \rightarrow CO_2$) to further reduce the carbon monoxide content. An alterative approach is to collect the hydrogen using a hydrogen separation membrane (before, during or after the WGS step).

Regardless of the fuel cell type or the fuel processing system design, there is a critical need for new fuel processing catalysts and catalytic structures. Desired attributes include improved resistance to impurities in the fuel, stability under transient (start-up, shut-down) conditions, and ruggedness. For smaller scale systems, high catalytic activity is desired to minimize overall system size and weight. Of particular importance is tolerance of the catalysts to the presence of sulfur in the fuel – to minimize the extent of sulfur removal required and to provide flexibility to the fuel cell system designers on the location of sulfur removal components. NexTech Materials currently is developing a number of catalytic materials and components to enable fuel cells to operate on hydrocarbon fuels. These include water-gas-shift catalysts, hydrocarbon reforming catalysts, sulfur adsorbents, and sensors for carbon monoxide and hydrogen sulfide. NexTech's work on sulfur tolerant hydrocarbon reforming and water gas shift catalysts is discussed in this paper.

Sulfur "Tolerant" Water Gas Shift Catalysts

Over the past several years, NexTech Materials has pursued the development of WGS catalysts based on ceria-supported precious metals. Our work has demonstrated that these catalysts offer several advantages compared to existing copper-based WGS catalysts: (1) operation over a wider range of temperature (up to 400ºC); (2) no need for activation prior to use; (3) no degradation upon exposure to air (non-pyrophoric); (4) capability for regeneration of deactivated catalysts by simple air-atmosphere annealing; and (5) availability of conventional washcoating technologies for supporting ceria-based catalysts on monoliths to improve ruggedness. NexTech has shown that performance of these catalysts is sufficient for the fuel processing application, and that volumetrically efficient WGS reactors can be produced using monolith-supported forms.

NexTech is extending its WGS catalyst formulations to sulfur tolerant versions under a project supported by the U.S. Navy's Ship Service Fuel Cell Program. Logistic diesel fuels (e.g., NATO F-76) have extremely high levels of sulfur (up to 10,000 ppm), which makes them difficult to work with using conventional fuel processing methods. One approach being pursued by the Navy is to reform this fuel with a sulfur tolerant catalyst, to increase hydrogen content with a sulfur tolerant WGS catalyst, and to collect the hydrogen with a sulfur tolerant membrane. Depending on the sulfur tolerance levels achieved by the catalysts and membranes, the size of desulfurization components can be greatly reduced with this approach. NexTech is focusing its efforts on WGS catalysts that are tolerant to high levels of H_2S (10-100 ppm) in the syngas feeds (N_2, CO, CO_2 and H_2).

Several sulfur-tolerant catalyst formulations have been identified and are being subjected to long-term testing. This testing is being conducted at relatively high temperatures (400 to 450ºC), because this is the temperature range where the membrane is targeted for operation. Specifically, NexTech is pursuing two strategies for the design of sulfur tolerant catalysts. The first is to improve robustness of high activity WGS catalysts, i.e., to increase their sulfur tolerance hopefully without compromising activity. The second approach is to increase the WGS activity of catalysts that are inherently tolerant to sulfur. These two approaches are exemplified by micro-reactor data shown in Figure 1. These data were obtained at 450ºC in a dry syngas composition (10% CO, 15% CO_2, 50% H_2 and 25% He), $H_2O/CO = 4.8$, and space velocity of ~150,000 cc/g-hr. Under these conditions, the "Type 1" catalyst was very active at low H_2S levels and decreased rapidly upon introduction of 50 ppm H_2S. Conversely, the "Type 2" catalyst exhibited stable WGS performance with 50 ppm H_2S during 300 hours of testing. Under these high-sulfur conditions, the catalyst of "Type 2" is the best option. Data obtained in a second set of tests at 400ºC in a syngas composition (15% CO, 10% CO_2, 50% H_2 and 25% He), $H_2O/CO = 2.6$, and 10 ppm H_2S are shown in Figure 2. Under these conditions, the "Type 1" catalyst is a better option and both types are clearly superior to commercial high-temperature shift catalysts.

Sulfur "Tolerant" Reforming Catalysts

NexTech also is developing hydrocarbon reforming catalysts for use with sulfur-containing fuels. Catalyst formulations being pursued include perovskite structured oxides and ceria-supported precious metals. A rapid screening test is used for initial catalyst evaluations, with comprehensive testing conducted on promising formulations. The screening test involves micro-reactor testing of methane partial oxidation and/or steam reforming reactions in feeds having sub-stoichiometric oxidant (where carbon formation is expected). By measuring the increase of pressure drop through the catalyst bed, an initial screen of coking resistance is obtained. An example of this test is shown in Figure 3 for a series of perovskite structured catalysts tested in the partial oxidation mode.

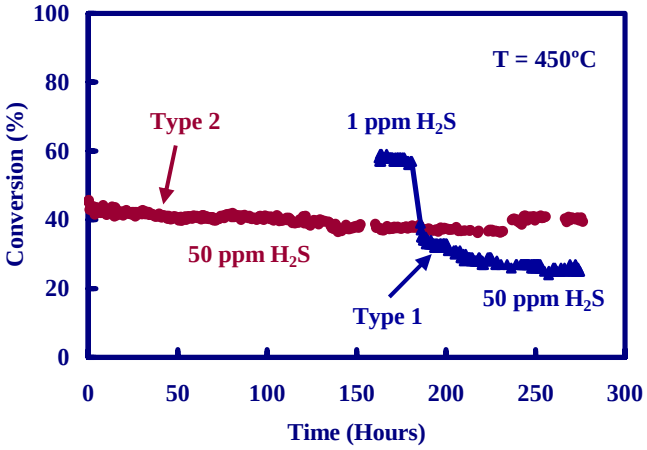

Figure 1. WGS performance of two types of sulfur-tolerant catalysts tested at 450ºC in syngas feeds of different H_2S contents.

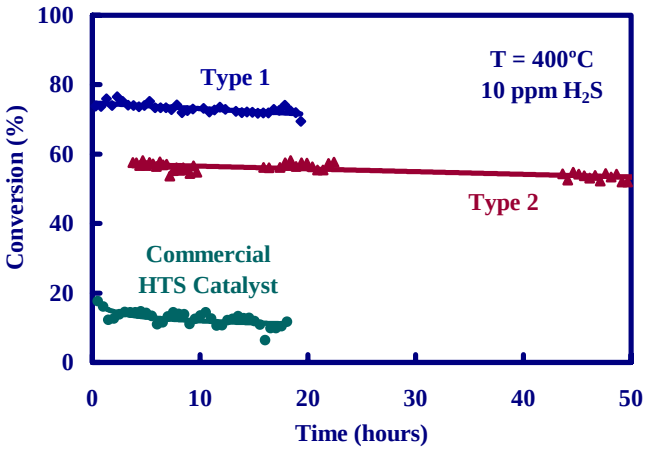

Figure 2. WGS performance of two types of sulfur-tolerant catalysts and a commercial catalyst tested at 400ºC (10 ppm H_2S).

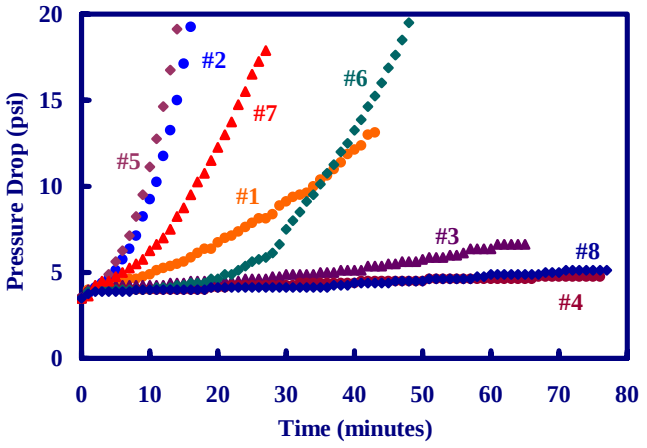

Figure 3. Pressure drop versus time for partial oxidation of methane at 700ºC with sub-stoichiometric oxidant (CH_4/O_2 = 3/1).

Based on the screening test results, several perovskite catalysts were selected for more comprehensive performance testing. These tests, typically 100-200 hours in duration, involved the measurement of methane conversions at temperatures of 650~800ºC under partial oxidation, steam reforming and autothermal conditions, with periodic exposures to H_2S (5-10 ppm levels). These perovskite catalysts were very effective for reforming of methane, especially when optimum synthesis methods were used (see Figure 4). Although none of the catalysts tested were completely immune to sulfur, three promising attributes were noted: (1) an onset period of a few hours after introduction of H_2S: and (2) relatively stable performance in the presence of H_2S after some activity loss; and (3) complete recovery of lost activity after H_2S was removed from the feed. An example of this behavior is shown in Figure 5.

Conclusions

The development of fuel processing catalysts that perform in the presence of sulfur in hydrocarbon fuels will greatly improve near term commercialization opportunities for fuel cell power generation systems. Two types of sulfur tolerant water gas shift catalysts have been demonstrated, with applicability depending on H_2S content and operating temperature. Several promising perovskite structured reforming catalyst formulations have been identified, and their sulfur resistance has been demonstrated for methane partial oxidation reactions. Future work at NexTech aims to extend the development of sulfur tolerant catalysts to different fuels and reforming reactions.

Acknowledgements. Funding for this work was provided by the Office of Naval Research (Contract No. N00014-04-C-0248) and by the National Science Foundation (Grant No. DMI-0419715).

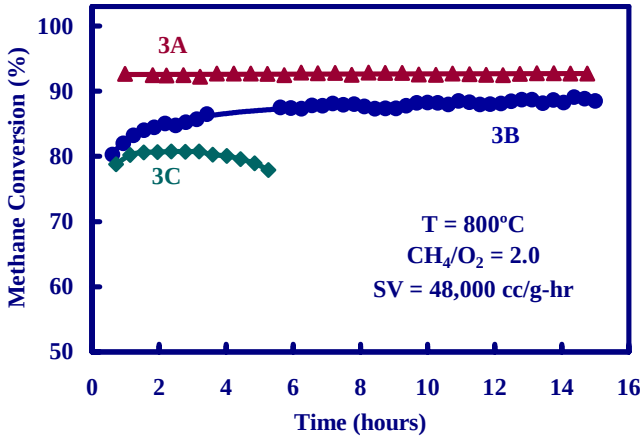

Figure 4. Effect of catalyst synthesis method on the stoichiometric methane partial oxidation for perovskite structured catalysts.

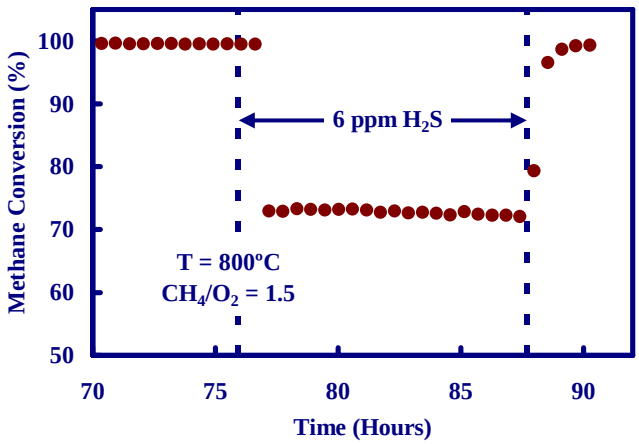

Figure 5. The effect of H_2S on methane conversion levels under partial oxidation conditions for a perovskite structured catalyst.

SURFACE STUDIES ON HIGHLY ACTIVE CeO_2 SUPPORTED CUPD BIMETALLIC CATALYSTS FOR THE OXYGEN-ASSISTED WATER-GAS-SHIFT REACTION

Elise B. Fox[*+], S. Velu, Karen Wilson[#] and Chunshan Song*

Clean Fuels and Catalysis Program
The Energy Institute
*Intercollege Graduate Program in Materials
Department of Energy and Geo-Environmental Engineering
Pennsylvania State University
209 Academic Projects Building
University Park, PA 16802, USA
[#]Department of Chemistry
University of York
Heslington, York, YO10 5DD, UK
[+]Presenting Author

Introduction

Reformed hydrocarbon fuels may become an important source of hydrogen for PEMFC's. In order to utilize these hydrogen sources, low levels of sulfur and carbon monoxide must be achieved. In a conventional fuel reformer for fell cell feed gases, the CO reduction steps of the high and low temperature water-gas-shift, and preferential oxidation can take up over 50% of the fuel cell systems volume and weight. In order to reduce this, the WGS and PrOx reactions are combined and performed in a single step, called oxygen-assisted water-gas-shift (OWGS) reaction. We recently developed a new series of highly active and less pyrophoric CuPd bimetallic catalysts supported on high surface area CeO_2 catalysts for the OWGS [1]. The catalyst containing about 30 wt % Cu and 1 wt % Pd has been found to be optimum in order to achieve high CO conversion close to 100 % around 230°C. The effect of temperature and space velocity on the catalytic performance has been evaluated. In the present study, we employed in-situ XPS and in-situ FT-IR studies over the $CuPd/CeO_2$ catalysts in order to understand the nature of active species involved in the OWGS reaction.

Experimental

Catalyst Preparation and characterization. The support CeO_2 was prepared by urea gelation method as described elsewhere and had a BET surface area of about 215 m^2/g.[5] Cu and Pd metals were deposited on the support surface using an incipient wetness impregnation (IWI) method, dried at 120°C overnight and calcined at 400°C for about 4 h using a heating rate of 2°C/min. TPR data were acquired on a Micromeritics AutoChem 2910 instrument. About 0.1 g of the catalyst was loaded in the reactor and heated in 5% H_2/Ar gas (25 cc/min) between room temperature and 500°C at a heating rate of 5°C/min. The H_2 consumption due to the reduction of constituent metal ions is monitored by a TCD detector equipped in the instrument.

XPS measurements were conducted at the University of York in a Kratos AXIS HSi instrument equipped with a charge neutraliser and a dual anode Mg K_α /Al K_α X-Ray source which was operated at 169 W. Spectra were acquired at normal emission with a pass energy of 20eV. Samples on the main stage can be heated up to 500°C under reactive gas exposure at pressures up to $1x10^{-7}$ torr. Higher pressure in-situ experiments were performed in the preparation chamber where pressures up to 0.1 bar and temperatures of 500°C were readily achievable.

Catalytic Studies. Oxygen-assisted water-gas shift reaction was performed at 180°C or 240°C in a fixed-bed down-flow reactor. A gas mixture containing 4% CO, 10% CO_2, 2% O_2 and balance (about 84%) H_2 was used as reactants. The CO/H_2O molar ratio was kept at 1/10. The effluent of the reactor was analyzed on-line using an Agilent 3000 A Micro GC equipped with thermal conductivity detectors with a CO detection limit of below 10 ppm. Prior to the reaction, the catalyst was reduced *in situ* at 225°C for 1h in H_2 flow.

Results and Discussion

XPS data of three samples, namely $Cu(30)Pd(0)/CeO_2$ containing only Cu without Pd, $Cu(0)Pd(1)/CeO_2$ containing only Pd without Cu and $Cu(30)Pd(1)/CeO_2$ containing both Cu and Pd in the unreduced as well as reduced form have been collected in order to understand the effect of Pd on the surface chemical properties of Cu/CeO_2 catalysts. The unreduced samples exhibited peaks corresponding to Cu^{2+}, Pd^{2+} and Ce^{4+}species in these samples. Upon reduction around 225°C, the Cu^{2+} and Pd^{2+} species are reduced mainly to their metallic states while Ce exists mainly in the Ce^{4+} state.

Figure 1 shows the XP spectra of reduced $CuPd/CeO_2$ catalysts in the Cu 2p and Pd 3d regions. The Cu 2p XP spectra exhibit sharp peaks around 932 eV for metallic Cu species. Significant differences in peak position and spectral intensity could be noticed in the Cu 2p spectra. Addition of Pd to the Cu/CeO_2 catalyst shifts the Cu $2p_{3/2}$ peak position towards lower BE by about 0.4 eV (932.4 eV for $Cu(30)Pd(0)/CeO_2$ and 932.0 eV for $Cu(30)Pd(1)/CeO_2$ catalysts) indicating that the reducibility of Cu is improved by the addition of Pd. This also leads to a decrease in intensity of the Cu 2p peak, suggesting that the surface dispersion of Cu is improved by the addition of Pd. The XP spectra collected in the valence band region, below 10 eV showed that Cu 3d bands are located close to the Fermi energy (E_F = 0) indicating that Cu is mainly involved in chemical interaction, converting CO into CO_2. The overall spectral intensity decreased upon addition of Pd, further supporting the core level observation that the Cu dispersion is improved by the addition of Pd. The XP spectra in the Pd 3d region indicate that the Pd is present mostly in Pd^0 state in the catalyst containing both Cu and Pd while significant amount of Pd^+ and/or Pd^{2+} is present in the catalyst without Cu. The presence of Cu helps retaining Pd in its metallic state. Thus, the existence of a synergistic interaction between Cu and Pd in the CuPd bimetallic catalysts supported on CeO_2 is clearly seen from the XPS data. The existence of Cu-Pd alloy on the surface of these Cu-Pd bimetallic catalysts could be responsible for the higher catalytic activity for CO oxidation [2].

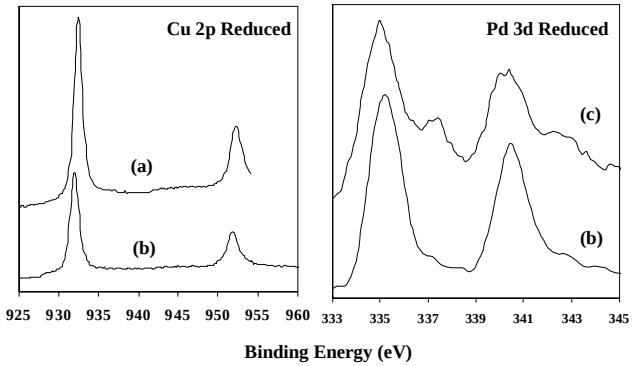

Figure 1. Cu 2p and Pd 3d XP Spectra of $CuPd/CeO_2$ catalysts; (a) $Cu(30)Pd(0)/CeO_2$, (b) $Cu(30)Pd(1)/CeO_2$, (c) $Cu(0)Pd(1)/CeO_2$

References
(1) Bickford, E. S.; Velu, S.; Song, C. S. Nano-structured CeO_2 supported Cu-Pd bimetallic catalysts for the oxygen-assisted water-gas-shift reaction *Catalysis Today* **2005**, *99*, 347-357.
(2) Hungria, A. B.; Iglesias-Juez, A.; Martinez-Arias, A.; Fernandez-Garcia, M.; Anderson, J. A.; Conesca, J. C.; Soria, J. Effects of copper on the catalytic properties of bimettallic Pd-Cu/(Ce,Zr)Ox/Al2O3 and Pd-Cu/(Ce,Zr)Ox catalysts for CO and NO elimination *Journal of Catalysis* **2002**, *206*, 281-294.

SYNTHESIS AND CHARACTERIZATION OF NON-NOBLE NANO-CATALYSTS FOR HYDROGEN PRODUCTION

Debasish Kuila*[1], Krithi Shetty[1], Wei Cao[2], Shihuai Zhao[3] Daniela Mainardi[4], and Naidu V. Seetala[5]

[1]Institute for Micromanufacturing/Chemistry, Louisiana Tech University, [2]Institute for Micromanufacturing, Louisiana Tech University, [3]Institute for Micromanufacturing, Louisiana Tech University, [4]Institute for Micromanufacturing/Chemical Engineering, Louisiana Tech University, [5]Department of Physics, Grambling State University

Introduction

Steam reforming is a process to produce hydrogen from organic sources with the aid of a catalyst. At present, there is no cost- and energy-efficient method for making hydrogen. Today, petrochemical plants generate millions of tons of hydrogen for different applications from methane for different applications. The expensive platinum catalysts require significant amounts of energy and produce 3 tons of carbon dioxide for each ton of hydrogen [1-5]. Coal gasification can produce considerable amounts of hydrogen and electricity due to availability of large size of coal deposits. However, energy necessary to sequester CO_2 is relatively expensive [6]. Of the many candidates being considered for hydrogen fuel sources, methanol and ethanol are readily available and currently being investigated [7-21]. Alcohols from biomass are easy to produce and safe to handle, store and transport.

A number of commercial and research-derived noble metals such as Pt, Rh, etc. with metal oxides, such as CeO_2, ZnO, MgO supports including more than one type of catalyst-support have been tested for hydrogen production from methanol and ethanol [7-10]. The performance is greatly influenced by the type of supports (CeO_2, Al_2O_3, SiO_2, ZrO_2, MgO or TiO_2) through interactions between catalyst and supports, with CeO_2 showing the highest selectivity to hydrogen. It has been speculated that a CeO_2 supported catalyst has a longer catalytic life time than that of Al_2O_3 [11]. Although a number of catalysts including Cu and Pd have shown promising results, problems with deactivation of the catalysts with an ensuing decrease in hydrogen and carbon dioxide and an increase in carbon monoxide production have been reported [9]. Currently, there is no proper understanding of these systems. In addition, the noble metal catalysts are expensive. Thus, fundamental research is necessary to find the optimized combination of catalyst and support for hydrogen production.

Microreactors have been used for production of hydrogen fuel for Proton Exchange Membrane (PEM)-based fuel cells by catalytic steam reforming of methanol [13]. However, they have not been used to explore the activity of catalysts for steam reforming. Advantages of micro-reactor systems include light weight and compactness, rapid heat and mass transport due to a large surface to volume ratio, and precise control of process conditions with higher product yields. The special emphasis of this project will center on non-noble metal catalysts for hydrogen production.

Experimental

Catalyst preparation. The silica supported Co or Ni catalysts were prepared by a sol-gel procedure developed in this laboratory.

Characterization. Scanning Electron Microscopy (SEM) associated with Energy Dispersive X-ray (EDX) from Amray 1830 instrument was used to investigate coating profiles and actual loadings of the nano catalysts. The specific surface area (SSA) of the silica encapsulated catalysts was characterized using Brunaur-Emmett-Teller (BET) method and Quantachrome NOVA 2000 analyzer. A Vibrating Sample Magnetometer (VSM) (880A Digital Measurement Systems) was used to study the magnetic properties of the catalysts at different stages.

Steam reforming of methanol. The catalytic reactions of steam reforming were conducted using a silicon based microreactor in the temperature range of 473-573 K under atmospheric pressure. Various flow rates in the range of 5-20 µL/min were controlled into the microreactors using a syringe pump. The parameters for reaction conditions were controlled using LabVIEW software. A cold trap separates out the gaseous products from aqueous methanol and water to calculate methanol conversion and thus also prevents the filament inside the mass spectrometer from high humidity. The gaseous products were diluted with helium and analyzed using a Mass Spectrometer (MS) (QMS 200 gas analyzer from Stanford Research Systems).

Results and Discussion

Characterization of silica sol-gel supported Co or Ni catalyst. The silica encapsulated Co or Ni was evenly coated in microchannels with nonuniform thickness. (Figure 1) This is due to the nature of the sol-gel process, generating pore structure of the catalyst support with high SSA, which is ~300 m^2/g from BETmeasurement. The EDX analysis shows that the Co catalyst loading is 7.85%, which is lower than intended loading of 12% due to catalyst preparation and deposition procedure.

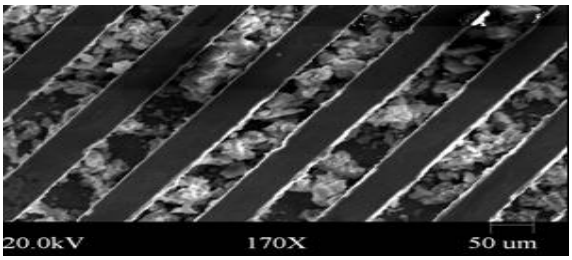

Figure 1. SEM image of Co/SiO_2 catalyst in a 50 µm channel-wide Si-microreactor

VSM studies of the as-deposited catalyst in microreactor show paramagnetic behavior mostly coming from the cobalt oxide (Figure 2). Hydrogenation of the catalyst reduces the oxide to pure metal, thus yielding ferromagnetic behavior. This ferromagnetic nature almost disappears in the post-catalyst due to the formation of Co carbide or carbonyl during the steam reforming reaction.

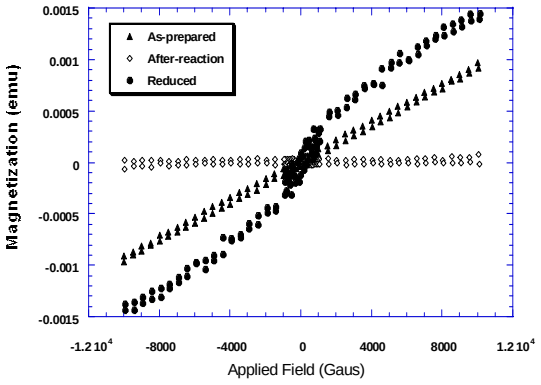

Figure 2. Magnetic studies using VSM of Co nano-catalyst: as prepared, reduced, and after steam reforming.

The saturation magnetization of the ferromagnetic component is used to estimate the catalyst activity in pre- and post-catalysts. It gives an estimate of the amount (~ 90%) of Co becoming inactive after the reaction.

Catalytic activity of steam reforming of methanol. The steam reforming of methanol was initiated at 473 K with the H_2O/CH_3OH ratio of 1, which has been reported in literature as the best conditions for steam reforming. The conversion of methanol declined as the flow rate was increased. But the flow rate had little influence on hydrogen production (Table 1).

Table 1. Steam reforming at 200°C with 1: 1 molar ratio of H_2O/CH_3OH.

Temperature (°C)	180	200	220	240	260	280	300
Methanol Conversion (%)	43.47	44.58	51.68	49.40	54.92	57.29	56.53
Hydrogen Percentage (%)	75.64	75.76	72.56	74.42	70.51	71.26	70.42
CO Percentage (%)	1.24	1.24	1.97	1.25	2.56	2.09	2.61

According to above results, higher methanol conversion is observed at lower flow rates. However, our mass spectrometer can not detect methanol when the flow rate is lower than 1 µl/min. Therefore, a fixed flow rate of 5 µL/min was chosen in our experiments to determine the influence of reaction temperature on both methanol conversion and selectivity to hydrogen (Table 2). The temperature for the experiments ranged from 180°C to 300°C and higher temperature yields a higher methanol conversion with a higher concentration of CO.

Table 2. Steam reforming at the flow rate of 5 µL/min with 1: 1 molar ratio of MeOH: H_2O.

Flow Rate (µl/min)	1.0	5	10	20	40
Methanol Conversion (%)	43.92	37.63	33.97	17.37	6.21
Hydrogen Percentage (%)	74.7	73.5	68.22	69.32	68.25

Preliminary results for Ni catalyst also show good trends and a conversion of 30% has been observed during the first few runs. Currently, we have developed a parallel array of microreactors to screen catalyst for Fischer-Tropsch (F-T) studies to make higher alkanes. This is also an ideal system for future hydrogen production studies due to significant decrease in catalyst development period with precise process control, flexible experiment operation and low operation/maintenance costs.

Computational studies

Computational studies are being conducted to gain a better understanding of the catalyst surface and mechanistic aspects of hydrogen production. The effect of nanoparticle size and temperature in the range of 300-1000 K at atmospheric pressure on SiO_2-supported Ni nanoparticles were investigated using molecular dynamics simulations. The annealing process of these nanocatalysts was simulated starting at a high temperature (1000 K), at which the system is fully equilibrated, and then successive simulations were run restarting always from the previous one until full equilibration was complete at 300 K. This procedure was further repeated for different nanoclusters sizes.

Preliminary results show clear differences in nanoparticles morphologies and structures depending upon the temperature of interest, and the characteristics of the liquid-solid transition in such nanoparticles. Nanoparticle surface characteristics, including exposed crystallographic phases, may play a key role in the catalytic activity and can be specially controlled and tailored by selecting a specific support. These simulations provide data needed to carry out more complete kinetic studies to simulate the complete steam reforming reactions taking place on the supported nanocatalysts.

Conclusion

The silica encapsulated Co or Ni catalysts were prepared using sol-gel method. Characterizations of the nano catalysts by SEM and EDX show even coatings of the silica supported catalysts in microchannels with lower loading than intended. The VSM studies showed transformation of Co magnetic properties at different stages. The highest conversion of methanol over Co catalyst is 57% at 280°C, at the flow rate of 5 µL/min, and 1: 1 molar ratio H_2O/CH_3OH, and much higher than that observed from the preliminary experiments over Ni catalyst (30%). Preliminary computational studies indicate that the crystallographic phases may be important for hydrogen production.

Acknowledgement. This work was supported by NSF-EPSCoR. Financial support in part from Pfizer Corporation is gratefully acknowledged.

*For Correspondence; Phone: 318-257-5121; Fax: 318-257-5104; dkuila@latech.edu

References

1. Mattos, L. V.; Rodino, E.; Resasco, D. E. *Fuel Processing Technology, 83* (**2003**) 147.
2. Matsumura, Y.; Nakamori, T. *Applied Catalysis A: General, 258* (**2004**) 107.
3. Takahashi, R.; Sato, S. Applied *Catalysis A: General, 273* (**2004**) 211.
4. Roh, H.; Jun, K. W.; Dong, W. S. *Journal of Molecular Catalysis A: Chemical, 181* (**2002**)137.
5. Yamazaki, O.; Tomishige, K.; Fujimoto, K. *Applied Catalysis A: General, 136* (**1996**) 49.
6. Energy Information Administration, unpublished file data of coal reserves data base (February 2004) available http://www.eia.doe.gov/pub/international/iea2002/table82.xls
7. Goula, M. A.; Kontou, S. K.; Tsiakaras, P. E. *Applied Catalysis B: Environmental, 49* (**2004**) 135.
8. Purnama, H.; Ressler, T.; Jentoft, R. E.; Soerijanto, H.; Schlogl, R.; Schomacker, R. *Applied Catalysis A: General, 259* (**2004**) 83.
9. Twigg, M. V.; Spencer, M. S. *Topics in Catalysis, 22*, 3-4, April (**2003**) 191.
10. Mizuno, T.; Matsumura, Y.; Nakajima, T.; Mishima, S. *Int. J. of Hydrogen Energy 28* (**2003**) 1393.
11. Zhang, X.; Shi, P. *Journal of Molecular Catalysis A: Chemical 194* (**2003**) 99.
12. Frusteri, F.; Freni, S.; Spadaro, L.; Chiodo, V.; Bonura, G. *Catalysis Communications 5* (**2004**) 611.
13. Pattekar, A. V.; Kothare, M. V. *Journal of Microelectromechanical Systems 13* (**2004**) 7.
14. Fatsikostas, A. N.; Verykios, X. E. *Journal of Catalysis, 225* (**2004**) 439.
15. Batista, M. S.; Rudye Santos, K. S.; Assaf, E. M. *Journal of Power Sources, 134* (**2004**) 27.
16. Srinivas, D.; Satyanarayana, C. V. V.; Potdar, H. S. Ratnasamy, P. *Applied Catalysis A: General, 246* (**2003**) 323.
17. Mariño, F. J.; Cerrella, E. G.; Duhalde, S. *International Journal of Hydrogen Energy, 23* (**1998**) 1095.
18. Men, Y.; Gnaser, H.; Zapf, R.; Hessel, V. *Catalysis Communications, 5* (**2004**) 671.
19. Bravo, J.; Karim, A.; Conant, T. *Chemical Engineering Journal, 101* (**2004**) 113.
20. Liu, Y.; Hayakawa, T.; Suzuki, K.; Hamakawa, S. *Applied Catalysis A: General, 223* (**2002**) 137.
21. Lwin, Y.; Daud, W. R. W. *International Journal of Hydrogen Energy, 25* (**2000**), 47.

REGENERABLE SORBENTS USED FOR THE REMOVAL OF SULFUR CONTAINING ODORANTS FROM WATER BEARING NATURAL GAS

Gőkhan O. Alptekin, Margarita Dubovik, Sarah J. DeVoss, and Robert Amalfitano

TDA Research Inc
12345 W. 52nd Ave
Wheat Ridge, CO 80033

Introduction

Fuel cells have the potential to revolutionize the way the power is produced and distributed, and distributed power generation is becoming a viable alternative to buying power from a central grid. However, there are still some hurdles to be overcome if fuel cells are to fully reach their commercial potential. One of the issues to be addressed is the need to provide an ample supply of high quality fuel to operate the fuel cells. Pipeline natural gas is the fuel of choice in distributed power generation systems because of its abundance and well-developed supply infrastructure. However, the natural gas contains sulfur impurities that can degrade the performance of the fuel cells. Although the majority of the sulfur in the natural gas is removed at the wellhead, some hydrogen sulfide (H_2S) and carbonyl sulfide (COS) exist as contaminants at low concentrations. In addition to the naturally occurring sulfur, pipeline gas also contains other organic sulfur species used as odorants. Because natural gas has no distinct odor, for safety reasons pipeline companies commonly odorize natural gas as it enters the transmission lines or local distribution facilities. These odorants allows detection of even minute leaks in the gas lines. Common odorants include mercaptans (such as ethyl, isopropyl, tertbutyl mercaptan), thiols (such as tetrahydrothiophene) and sulfides (such as dimethyl or diethyl sulfide). The concentration of sulfur in odorized natural gas can be as high as 10-15 ppm on volume basis.

Fuel cells, however, require clean feed streams with very low levels of sulfur and other impurities. Sulfur poisons the anode catalysts for both high and low temperature fuel cells. The problem is most severe in polymer electrolyte fuel cells (PEMFC), both because they operate at low temperature, and their platinum group catalysts are highly susceptible to sulfur poisoning. Sulfur also degrades the performance of the high temperature solid oxide fuel cells (SOFCs). A recent study by Siemens Westinghouse Power Corporation [1] shows that the performance of their fuel cell drops about 15% in the presence of 1 ppmv sulfur in the fuel. Although this poisoning effect is reversible, long-term stable electrochemical performance of the SOFCs requires sulfur concentrations to be reduced to sub ppmv levels.

In large central stations, sulfur removal is carried out upstream of the fuel cell with a two-step process consisting of hydrodesulfurization of organic sulfur species to H_2S and subsequent H_2S removal with a sorbent. However, this method is not practical for small-scale residential units. Most fuel cell manufacturers prefer a low temperature adsorbent that can directly remove organic sulfur from natural gas in a single step. A successful sorbent must meet a number of requirements. First of all, it must exhibit a high sulfur adsorption capacity to reduce the size of the sorbent bed and decrease the replacement frequency of the sorbent. It has to be low cost, so that it is affordable by households. It must reduce the total sulfur concentration of the fuel to ppb levels to ensure maximum protection for the fuel cell catalyst. It must operate in a passive manner and should not catalyze any undesirable side reactions or alter the composition of the gas by adsorbing hydrocarbons. It must tolerate other natural gas contaminants such as the heavy hydrocarbons, CO_2 and humidity. Finally, it should be easy to dispose of. The sorbent itself should be easy to handle and should not pose any toxicity, flammability or pyrophorocity problems.

TDA Research, Inc. is developing a passive adsorbent for the ambient temperature desulfurization of natural gas. This paper summarizes the test results showing the effects water vapor on sorbent performance and the regenerability of the sorbent.

Experimental

Testing System. The sorbent performance was measured in an automated bench-scale test unit. In this setup, the reactor cell consists of a quartz tube that contains a frit in the middle to support the pellets. We were able to test 0.5 to 2.0 g of sample (1/8" pellets were crushed into 1-5 mm size to be tested). The reactor was inserted in a tube furnace to provide heating as needed. All gas flows were controlled with electronic mass flow controllers. To introduce organic sulfur species we used calibrated gas cylinders that contain mixtures of odorant species with natural gas. A valve system was used to direct gases to a reactor by-pass line to make accurate measurements of the feed gas. All system components were made of either quartz, Teflon or Silcosteel (steel lines with a special glass coating) to minimize the adsorbtion of sulfur on the system components. All testing was done at near ambient pressure (3 psig). The apparatus is fully automated and can run without an operator for long periods of time, including overnight.

Sulfur Analysis. For the analysis of sulfur compounds we used a gas chromatograph equipped with a flame photoionization detector that is selective to sulfur species. The capillary column used to separate the odorants is a RTX-1, 30 meter, 0.53 mm ID, with 7.0 μm film thickness manufactured by Restek Corporation. Our detection limit was approximately 0.1 ppmv. The correlation between the amount of sulfur-bearing gases passed over the sorbent and the amount of sulfur accumulated in the bed allowed us to identify the effectiveness of the sorbent and provided an independent check on our analytical methodology.

Hydrocarbon Analysis. In these tests, we used simulated natural gas. This gas mostly consists of lower alkanes from methane to hexane, with some branched hydrocarbons such as the iso-butane or neo-pentane at representative concentrations. The gas also contained some nitrogen and CO_2. We used a GC equipped with a thermal conductivity detector to measure the concentration of the hydrocarbon species throughout the test.

Results and Discussion

Effect of Water Content of Natural Gas. In the screening tests, the samples were tested using certified gas mixtures of simulated dry pipeline gas. However, typical U.S. pipeline natural gas may contain up to 155 ppmv of water vapor (~7 lbs of water per million cubic foot of natural gas). It is anticipated that the competition by water vapor for adsorption sites will reduce the sulfur capacity of activated carbon, zeolite-based sorbents in real world applications due to their high affinity to water. Therefore, some of the samples were evaluated using a gas stream containing 45 ppmv water vapor with all other gas concentrations remaining identical (i.e., 12.3 ppmv DMS, 8.9 ppmv TBM and 8.9 ppmv THT at a GHSV of 60,000 h^{-1}). Figure 1 shows the effect of water vapor on the performance of Norit RGM3 Activated Carbon, unmodified zeolite-X (Grace) and TDA's SulfaTrap™ sorbent. The presence of water reduced the sulfur adsorption capacity of all sorbents. The capacity of the zeolite-X is reduced the most by approximately 83%, showing zeolite-X's high affinity for the water vapor. The water most likely adsorbs on the surface of the sites, competing with the sulfur. As shown in Figure 1, the capacity of the SulfaTrap™ sample is also reduced in the presence of 50 ppmv water vapor. However,

the competition with water vapor was less of a problem for the SulfaTrap™ sorbent.

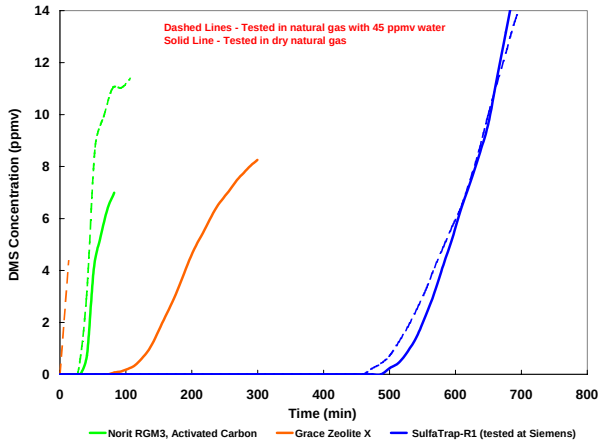

Figure 1. Effect of water on sulfur adsorption capacity of selected adsorbents. The samples were tested at 22°C and a pressure of 3 psig, gas hourly space velocity (GHSV) of 60,000 h^{-1}, with 12.3 ppmv dimethyl sulfide (DMS), 8 ppmv tert-butyl mercaptan (TBM) and 8 ppmv tetrahydrothiophene (THT).

Cyclic Tests. SulfaTrap™ sorbent can be regenerated with a mild temperature swing. The cyclic sulfur adsorption capacity of the sorbent was measured for ten consecutive adsorption/regeneration cycles. Each cycle started with a feed analysis, followed by sulfur adsorption. Once the test was completed, the sorbent bed was heated for the regeneration. These regenerations were carried out in either hydrogen or natural gas (both of which will be available on-site as fuel) containing no odorants. After the regeneration is complete (no further sulfur release was observed), the sorbent was cooled down to room temperature. The next cycle was then started. Figure 2 shows the DMS breakthrough curves for the ten cycle test. The sorbent maintained a stable total sulfur capacity and the DMS capacity of through this ten cycle test. As shown in Figure 3, the sorbent exhibited slightly higher sulfur adsorption capacity following the regenerations carried out in hydrogen show. The loss of capacity due to the natural gas regeneration can be even regained when hydrogen is used for regeneration.

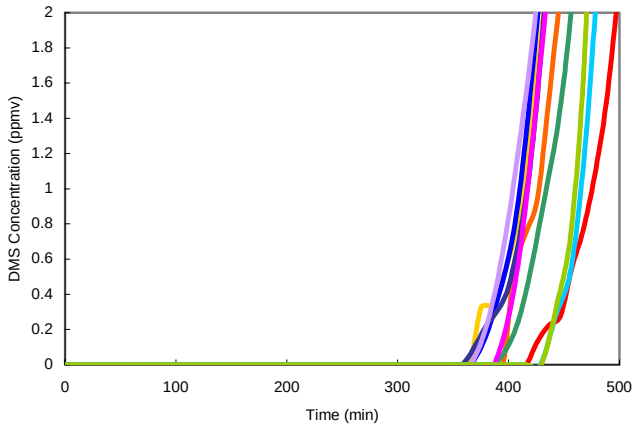

Figure 2. DMS breakthrough profiles during the 10-cycle test at 22°C, 3 psig, GHSV= 60,000 h^{-1}, with odorant inlets of 12.3 ppmv DMS, 8 ppmv TBM and 8 ppmv THT.

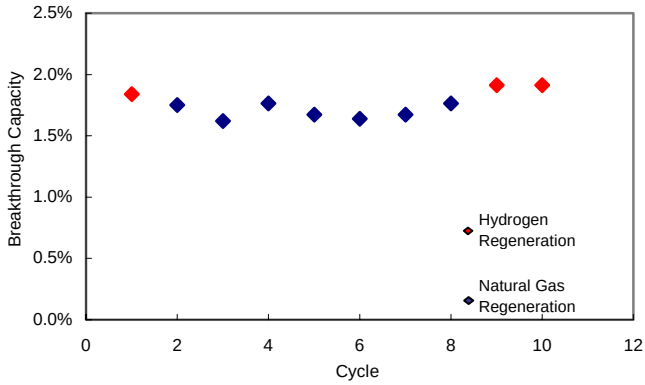

Figure 3. Sulfur capacity of the sorbent during the 10-cycle test at 22°C, 3 psig, GHSV= 60,000 h^{-1}, with odorant inlets of 12.3 ppmv DMS, 8 ppmv TBM and 8 ppmv THT. The capacity is defined as lbs of sulfur adsorbed per lb of sorbent.

Conclusions

A new sorbent was developed for removing sulfur-bearing odorants from natural gas at ambient temperature. SulfaTrap™ sorbent can achieve high sulfur capacity even in the presence of water. It was also shown that the sorbent can successfully be regenerated in either sulfur free natural gas or hydrogen.

Acknowledgements

We wish to thank Mr. Gordon Israelson, of Siemens Westinghouse Power Corporation for discussions. The funding for this research was provided by DOE Phase II SBIR Grant, Contract No. DE-FG02-03ER83795. The authors also thank Mr. Donald Collins of NETL, DOE and Mr. Norman Holcombe of NETL, DOE.

References

(1) Israelson, G.; *Journal of Materials Engineering and Performance*, Vol. 13(3), June **2004**

MASS TRANSFER STUDY OF HYDROGEN SULFIDE REMOVAL FROM REFORMATS WITH MICROFIBER ENTRAPPED ZnO / SiO_2 SORBENTS FOR FUEL CELL APPLICATION

H.-Y. Yang N. Sathitsuksanoh, Y. Lu, B. J. Tartarchuk

Department of Chemical Engineering
Auburn University
Auburn, AL 36849

Introduction

A significant challenge facing Fuel Cell applications is the development of on-site multi-step reformation technologies utilizing high energy density commercial-grade hydrocarbon fuels. So far, most designs have adopted packed bed reactors, which do not scale well with the small modular nature of fuel cells. Packed beds of catalyst/sorbent pellets of one to five millimeters in diameter suffer from high intraparticle mass/heat transfer. Mass transfer may be ameliorated by decreasing the particle size and increasing the face velocity, which in turn causes the high pressure drop and bypassing in packed bed. On the other hand, catalyst/sorbent pellets are not likely to withstand mechanical shaking in many applications (such as portable electric devices, propulsion devices, etc.); powdered catalysts may clump in a way that leads to fluid bypassing. Bare metals and catalysts washcoats have been used to avoid one or more of these problems [1-4], but surface areas per unit reactor volume have remained unacceptably low.

In this paper, we describe our research effort towards small, efficient, lightweight fuel processors based on microfibrous media technologies developed at Auburn University [5-12]. Microfibrous media carrier can be used, with large surface to volume ratios, to entrap micro-sized sorbent and/or catalyst particulates while withstanding considerable shaking and avoiding bypassing. This generic approach can also improve contacting efficiency, and promote regenerability while make more effective (cassette type) design of reactor possible [13-15].

Bulk H_2S removal is a key step of the fuel processor in ensuring the activity of various cleanup catalysts and high value membrane electrode assemblies. To accomplish this goal, the sintered glass fiber media entrap micro-sized ZnO/SiO_2 sorbent particulates was prepared. In this paper, the basic mass transfer study about this sorbents has been conducted

Experimental

Sorbents Preparation. Sintered glass fiber entrapped 150-250 mm (dia.) SiO_2 ($300m^2/g$, Grace Davison) support particulates were fabricated by regular wet layer paper-making/sintering procedure [5-12]. ZnO was then placed onto the supports by incipient wetness impregnation. 6g of glass fiber chops, and 0.7g of 30-60 mm (dia.) cellulose (100-1000 μm in length) were added into about 5L water and stirred at 50Hz to uniform suspension. The produced suspension and 12g SiO_2 were added into the headbox of the 6-inch (dia.) circular sheet former under stirring. A 6-inch circular preform was then formed by draining followed by pressing at ~ 400kNm-1 and drying in air at ~110°C. The As-prepared perform was directly sintered in air for 30 min at 925 °C, while burning off the celluloses. The sintered glass fiber entrapped SiO_2 particulates comprises 3.0 vol% of glass fibers, 45 vol% of 150-250 μm (dia.) SiO_2 particulates, and 52 vol% voidage. To place the ZnO onto the support, the as-prepared microfibrous entrapped SiO_2 paper was immersed into a ZnO sol-gel for 10min. The ZnO sol-gel was prepared by adding 70ml $NH_3 \cdot H_2O$, 42g $(NH_4)_2CO_3$, and 66g $Zn(Ac)_2 \cdot 6H_2O$ in series into 56ml water under vigorously stirring. The paper was subsequently removed from the ZnO sol-gel, drained under vacuum, and calcined at 80°C→ 100°C→ 120°C→ 140°C→160°C→ 180°C in air and hold for 20min at each temperature point. The final composite sorbent product had a ZnO loading around 20wt% (including the mass of the glass fibers).

For comparative study, ZnO/SiO_2 sorbent without microfiber was prepared by the impregnation as mentioned above; commercial ZnO sorbent (3/16' ' pellet, 25m2/g, 90wt%ZnO) from Sud Chemie was crushed and sieved into desired particle size for comparative study use.

Apparatus and Equipments. The H_2S removal tests were conducted in a fixed bed quartz reactor (9mm id.).The challenging model reformat gas contains 2% H_2S (balance H_2) (Airgas,USA). In regeneration cycle, the household air was applied to convert ZnS to ZnO at 600 °C. A Gas Chromatograph (GC S-500, Gow-Mac, USA) was used to analyze the H_2S concentration in outlet gas.

Results and Discussion

Particle Size Effect. It is believed that sorbent of small size can enhance the intraparticle mass transfer, thus improves the utilization. In this study, Sud Chemie ZnO sorbent pellets were crushed and sieved into desired particle sizes. The comparison between the performance of ZnO/SiO_2 and Sud Chemie sorbents is shown in **Figure 1**. In each experiment, 0.18 g effective ZnO was loaded. Reactor temperature kept at 400 °C and face velocity 1.28 cm/s. The only difference is the particle size. It is clearly illustrated that the breakthrough curves shift right and give sharper breakthrough curves and higher capacities with the decrease in sorbents size. This is because smaller particles offer larger surface, which in turn means more sorbents may be accessible to challenge gas, assuming challenging gas can diffuse through the same distance d in the spherical sorbents particles, where d is less than the size of particles in Sud Chemie cases. If the size of ZnO particles is less than d, then theoretically all ZnO could be consumed by H_2S, which will only demonstrate a step at the theoretical saturation time in the breakthrough curve. Although the particles of this size are impracticable due to the drastic increase in pressure drop, the particulates could be supported on other particles with reasonable size. This is an idea to get rid of the intraparticles mass transfer resistance that suffers almost all packed beds. Actually, through the impregnation process, nanosized ZnO was dispersed on the silica particles [16]. As expected, the silica particle impregnated with nanosized ZnO demonstrates the sharpest breakthrough curve and the breakthrough capacity is twice that of Sud 40-60mesh. For convenience, the breakthrough was defined at the point that the outlet concentration reached 1% inlet concentration (C_0).

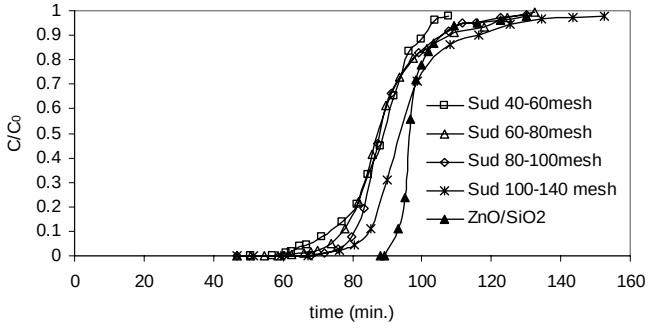

Figure 1. Breakthrough curves of Sud Chemie Sorbents with different size and ZnO/SiO_2 sorbents

External mass transfer study. In this study, the ZnO/SiO_2 sorbent is tested at 400 ^oC with challenge gas concentration (C_0) of 2%. In he first experiment, 0.1 g ZnO/SiO_2 (ZnO loading ratio 19%) sorbent was loaded and the face velocity is about 1.28 cm/s. In each of the following experiments, the weight of sorbent loaded and face velocity was twice of these in former experiment, thus the resident time was maintained unchanged, so did the theoretical saturation time. The breakthrough curves of /SiO_2 at different face velocities is shown in **Figure 2**. The breakthrough cure of glass fiber entrapped sorbent (GFE) with 0.019 g ZnO loaded at the face velocity of 1.28 cm/s is also shown for comparison.

All the breakthrough curves pass around the same point, which indicates the consistency of the theoretical capacity. It is a clear trend that the breakthrough curves become sharper with the increase in face velocity of challenge gas. For convenience, the breakthrough point was defined at 1% of inlet concentration. The capacity of sorbents in each experiment was calculated. As shown in **Figure 3**, the capacity at breakthrough increases significantly in low face velocity range. While, after the face velocity reaches 5 cm/s, the capacity is slowly approaching 0.37, about 90% of the theoretical capacity, which suggests that the unutilized ZnO is less than 10%. The breakthrough curve of glass fiber entrapped sorbents shows the capacity at breakthrough increases about 50% form the experiment m:V, though in both cases, the same type of sorbent (ZnO/SiO_2) with the same amount of ZnO had been loaded and . The only explanations for this improvement could be the enhancement of external mass transfer due to the glass fiber media.

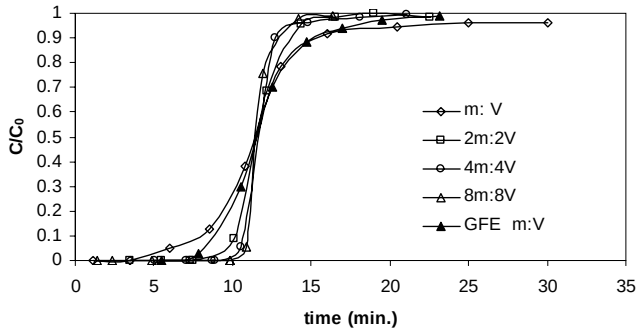

Figure 2. The breakthrough curves of ZnO/SiO_2 at different face velocities (C_0=2%, reactor temperature 400 ^oC).

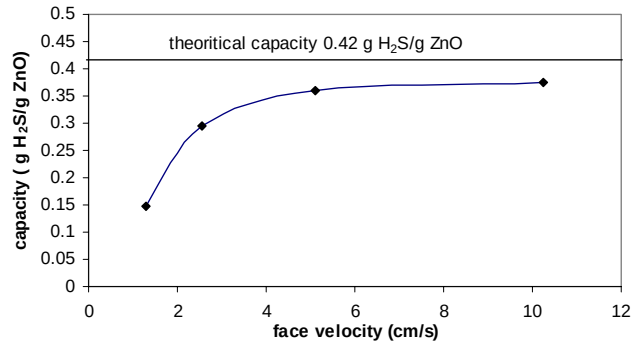

Figure 3. The breakthrough capacity of sorbent at different face velocities.

Due to the fast gas diffusion at high temperature, the improvement of microfiber media was not significant. It is known that the diffusivity decrease exponentially with the decrease of temperature. Thus, a series of experiments at room temperature was conducted. In these experiments, the challenge gas was fed at the same rate 23 ml/min, while the face velocity was about 0.51 cm/s. In each experiment, about 0.019 g ZnO was loaded. The comparison between the performance of ZnO/SiO_2 and ZnO/SiO_2 entrapped in glass fibers or glass mixtures of different fiber diameters was shown in **Figure 4**. Here there is a clear distinction in the performance of ZnO/SiO_2 particles and GFE. The hump in the breakthrough curve of former indicates that is a mass transfer dominated process, since the same sorbents entrapped in microfibers demonstrated much sharper breakthrough curves. Moreover, the fiber diameter also affected the mass transfer. The breakthrough curve of sorbents entrapped in the fiber with larger size, say 14μm, is not as sharp as that of smaller size, though this difference becomes not significant especially when the fiber diameter is less than 14μm.

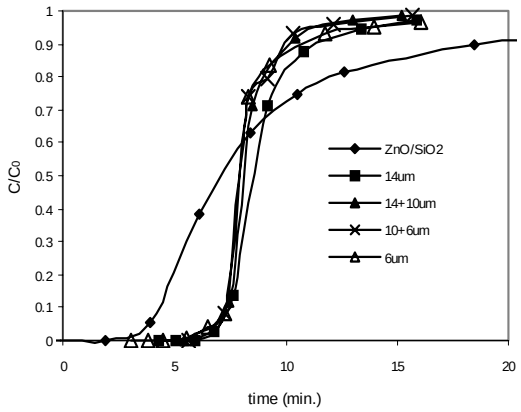

Figure 4. the performance of ZnO/SiO2 and ZnO/SiO2 entrapped in glass fibers of different diameters at room temperature.

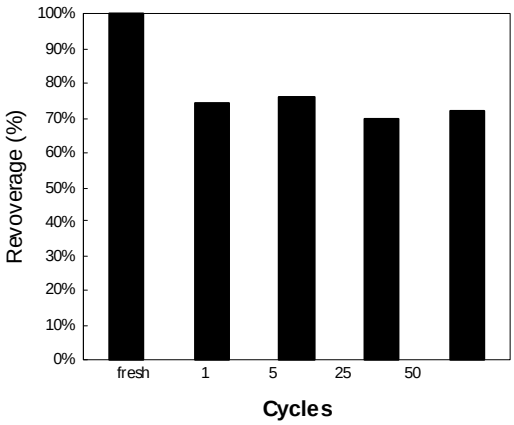

Figure 5. absorption/regeneration cycle test results over the GFE ZnO/SiO2 sorbents (absorption temperature 400 ^oC, regeneration at termperature 600 ^oC for 1 hour; define recoverage as the ratio of capacity of regenerated sorbent to that of fresh sorbent).

Regeneration. It is clear that the microfibers are able to enhance the external mass transfer thus improve the sorbents performance in the low concentration H_2S removal; ZnO nanosized particulates supported by SiO_2 can minimized the intraparticle mass transfer resistance. It is undoubted that it will also demonstrate outstanding performance in regeneration cycles, where oxygen, instead of H_2S in absorption case, diffuses in the sorbents. As shown in **Figure 5**, the regenerated sorbents have steady capacities which are around 75% of the capacity of fresh ones. From the mass transfer study of glass fiber

entrapped ZnO/SiO_2 sorbents, it is clear that the combination of these microfiber media nano-dispered ZnO on SiO_2 has offered a nice solution to the low concentration H_2S removal in onsite fuel processor.

Acknowledgment

Financial support from U.S. Army (DASG 60-00-C-0070) is gratefully acknowledged.

References

1. McCreedy, T. Trends Anal. Chem., 2000, 19, 396.
2. Srinivasan, S.; Hsing, I.M.; Berger, P.E.; Jensen, K.F.; Firebaugh, S.L.; Schmit, M.A.; Harrold, M.P.; Lerou, J.J.; Ryley, J.F. AIChE J., 1997, 43, 3059.
3. Watanabe, K.; Sakairi, M.; Takahashi, H.; Takahiro, K.; Nagata, S.; Hirai, S. J. Electrochem. Soc., 2001, 148, B473.
4. Wu, X.; Weng, D.; Xu, L.; Li, H. Surf. Coat. Technol., 2001, 145, 226.
5. Tatarchuk, B. J.; Rose, M. F.; Krishnagopalan, A.; Zabasajja, J.N.; Kohler, D. US Patent 5,304,330, 1994; US Patent 5,080,963, 1992.
6. Overbeek, R. A.; Khonsari, A. M.; Chang, Y.-F.; Murrell, L. L.; Tatarchuk, B. J.; Meffert, M. W. US Patent 6,231,792, 2001.
7. Tatarchuk, B. J. US Patent 5,096,663, 1992; US Patent 5,102,745, 1992.
8. Cahela D. R.; Tatarchuk B. J. Catal. Today, 2001, 69, 33-39.
9. Marrion, C. J.; Cahela, D. R.; Ahn, S.; Tatarchuk, B. J. J. Power Sources 1994, 47, 297-302.
10. Kohler, D. A.; Zabasajja, J. N.; Krishnagopalan, A.; Tatarchuk, B. J. J. Electrochem. Soc. 1990, 137(1), 136-141.
11. Ahn, S.; Tatarchuk, B. J. J. Appl. Electrochem. 1997, 27, 9-17.
12. Meffert; M. W. Ph.D. thesis, Auburn University, Auburn, AL, 1998.
13. Harris, D. K.; Cahela, D. R.; Tatarchuk, B. J. Composites, Part A: Applied Science and Manufacturing 2001, 32A(8), 1117-1126.
14. Lu, Yong; Tatarchuk, B. J. 226th ACS National Meeting, New York, NY, Sept. 7-11, 2003, CATL-042.
15. Lu, Yong; Tatarchuk, B. J. AIChE 2003 National meeting, San Francisco, CA, November 16-21, 2003, 331b.
16. Lu, Yong, Chang, B.-K., Yang, H.Y. Tatarchuk, Bruce J., ASM International, Columbus, OH, October 19, 2004 - 10:30 AM FUEL 4.5

INTEGRATED WATER GAS SHIFT (WGS) Pd MEMBRANE REACTORS FOR COMPACT HYDROGEN PRODUCTION SYSTEMS FROM REFORMING OF FOSSIL FUELS

Ying She, Zissis Dardas, Mallika Gummalla, Thomas Vanderspurt, Sean Emerson

United Technologies Research Center, 411 Silver Lane, East Hartford, CT 06108

Introduction

United Technologies Research Center (UTRC) is developing integrated Pd Membrane reactors for H2 production through reforming of fossil fuels. This is because, depending on the application, fuel & system design requirements, Pd membrane modules can be integrated in the reformer (catalytic steam reformer) or the Water Gas Shift (WGS) reactor, thus eliminating all the reactors, major part of the multiple heat exchangers and the air mixers in the traditional fuel processing system for H2 generation, down steam of the reactor that they are integrated with.

Metal supported tubular Pd membranes have high modularity and thus can be easily scaled up to any system capacity while they do not employ components with high reliability debits like rotating valves in high time frequency, as is the case for Pressure Swing Adsorption. This approach results in significant system cost savings and controls simplicity (thus higher system reliability) due to system simplification through component elimination.

Results and Discussion

Detailed system and reactor modeling, analysis, simulation, sensitivity analysis, parametric trade off & optimization studies were completed for an on board fuel processing system integrated with an ambient pressure 50 kWe PEM fuel cell stack and balance of plant. Parametric studies for the Pd membrane WGS reactor included reformate flow rate, composition, inlet temperature and pressure, sweep gas inlet temperature & flow rate, Pd membrane thickness, and tube support diameter, length and number of tubes. For example, Fig. 1 shows the influence of the inlet WGS reactor pressure on hydrogen recovery. As expected, hydrogen recovery increases with the increase in the pressure. Proprietary WGS catalyst kinetics integrated with mass & heat transfer processes were utilized to estimate require WGS catalyst volume. The optimum reactor & system design configuration and operating parameters were identified and the resulting system design had 6 points higher efficiency than the baseline design that does not employ a membrane reactor.

Significant accomplishments in Pd membrane permeance, selectivity & stability were demonstrated by the synthesis effort under development at UTRC. As shown in Fig. 2, hydrogen permeance & H_2/N_2 selectivity values with a proprietary synthesis approach based on electroless plating over modified porous stainless steel supports are ~50 m^3/m^3-hr-$atm^{0.5}$ and 150:1, respectively, with no evidence of performance deterioration for more than 300 hrs in hydrogen at temperatures in the 350-400 ^oC regime.

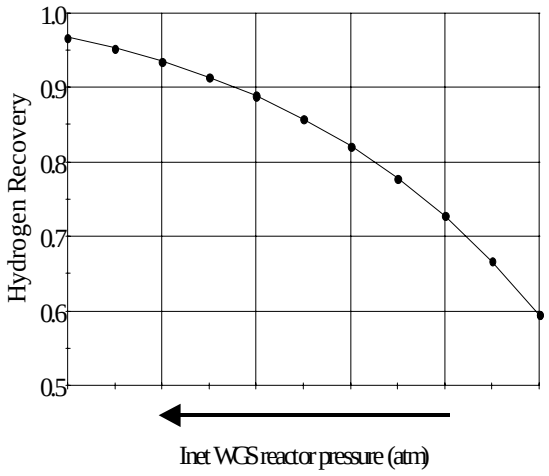

Figure 1. Effect of the inlet WGS reactor pressure on hydrogen recovery

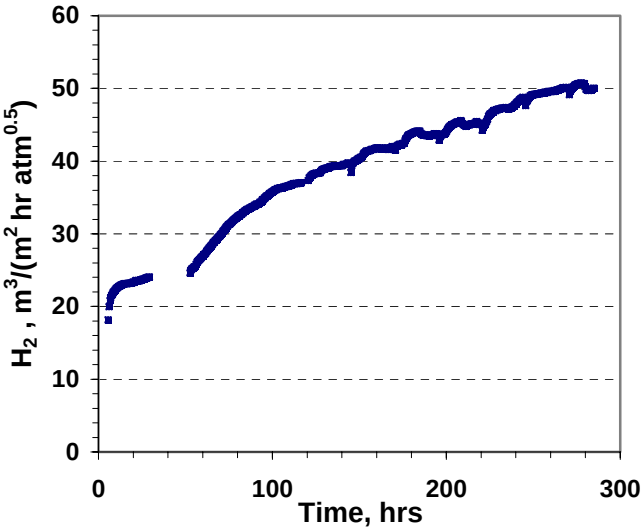

Figure 2. Hydrogen performance as a function of time

IN SITU FT-IR STUDY OF THIOPENE ADSORPTION AND REACTIONS ON SULFIDED Mo CATALYSTS

Dong Liu, Xue Kong, Zongxian Wang and Guohe Que

State Key Laboratory of heavy oil processing, University of Petroleum, Dongying, Shandong 257061, China

Introduction

Molybdenum based catalysts play an important role in the hydroprocessing of petroleum, and accordingly numerous studies have been made to clarify the surface structure and active sites by using infrared spectroscopy [1-5]. It is generally accepted that the sulfur vacancies is the active sites of HDS. The number of active sites on sulfide catalysts has typically been estimated by CO chemisorption [6,7], the HDS activity of sulfided molybdenum catalysts has been shown to correlate with both their CO and O_2 chemisorption capacities [8-10], the probe molecules selectivel adsorb on coordinately unsaturated Mo sites located on the edge planes of MoS_2 crystallites which are thought to be the active sites for hydrodesulfurization [11]. But the spectra of adsorbed CO on sulfided catalysts can only be found at low temperature, the results shows gap from real reactivity. NO can adsorb more easiely on sulfide catalyst at room temperature, little is known about the sites on which NO adsorb and what the relationship is between these adsorption sites and the active sites for hydrodesulfurization. The purpose of the current study is to investigate the relationship between the NO chemisorption sites and thiophene HDS activity using IR spectroscopy on sulfided Mo catalysts.

Experimental Section

Sample preparation: Two kinds of laboratory prepared catalyst (denoted by Cat.A and Cat.B) and Commercially available MoS_2 powders (denoted by Cat.C) were used in the present study. Cat.A was prepared by sulfurization of 15wt%MoO_3 / ɣ-Al_2O_3 in a stream of H_2S/H_2 gas mixture at 673K for 4h, MoO_3 / ɣ-Al_2O_3 was prepared by impregnation of ɣ-Al_2O_3 with aqueous solutions of ammonium heptamolybdate, following impregnation, the catalyst was calcined for 4h in air at 773K. Cat.B was prepared by the following method: aqueous solutions of ammonium heptamolybdate was scattered in gas oil well-proportioned, $(NH_4)_2S$ was introduced into the system, after sufidation keeping the temperature at 403K for 1h in a stream of N_2 to remove the water, the gas oil was displaced to high-pressure kettle and react in H_2 ambience at 693K for 1h, the toluene-insoluble distance was separated and then the sulfided water-solubility dispersed molybdenum catalyst attained.

Infrared Spectroscopy Measurements: Infrared spectroscopy measurements were carried out in a quartz cell. Catalyst samples were pressed into a self-supporting circular wafer with a diameter of approximately 13mm, and mounted on the sample holder, diagram of in situ infrared system shows in Fig1, and the quartz cell has been described in detail elsewhere [12]. A small well under the edge of the sample contained a thermocouple used to monitor the temperature of the system. The heating sector and the thermocouple are associated with temperature-programmed instrument to control the temperature of the system. IR spectra acquisition was accomplished using Nicolet Magna-750 Fourier transform-infrared spectrometer and consisted 60scans of the region of 4000-1200cm^{-1}, which took approximately 1min to acquire.

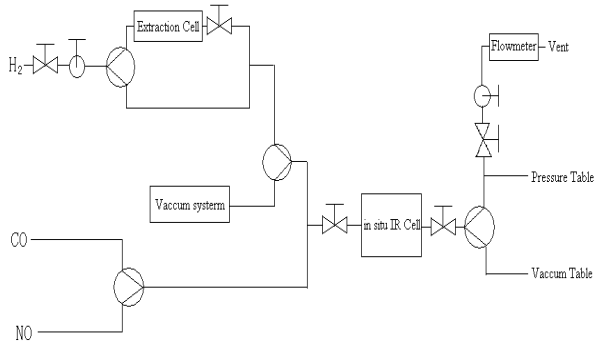

Fig1. Flow Diagram of In-situ FT-IR System

Depending upon the experiment, background spectroscopy was acquired for the wafer in UHV at corresponding temperature. After the catalyst exposed to pretreatment, NO was introduced into the cell and keeping the pressure of NO 0.08MPa for 1h at room temperature, outgassing about 5min and following acquisition of the IR spectrum of adsorbed NO on catalysts.

Thiophene Adsorption and HDS Activity Measurements: Thiophene Adsorption and HDS Activity Measurements were determined also in the stainless-steel cell as previous. H_2 carried the solid thiophene into the cell and the pressure of H_2/thiophene was 0.08MPa, HDS reactions were carried out at 673K for 1h in the cell. The infrared spectroscopy was recorded during the temperature increasing.

Results and Discussion

Infrared Spectroscopy of Adsorbed NO: The IR spectra of NO chemisorbed on Cat.A, Cat.B and Cat.C are displayed in Fig2.

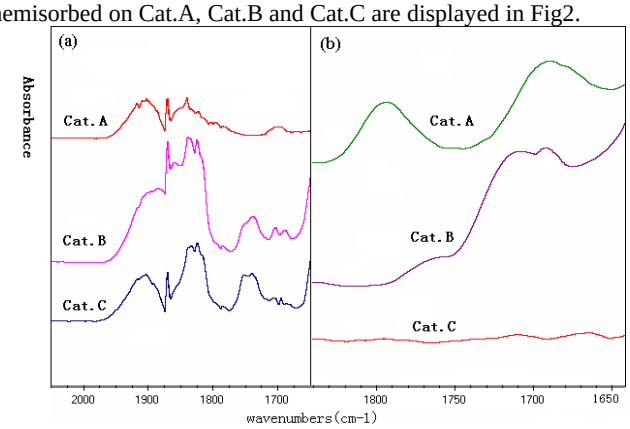

Fig2. IR spectra of NO adsorbed on Cat.A, Cat.B and CatC. (a) in 0.08MPaNO and
(b) after outgassing at room temperature.

The spectra of different catalysts differ in intensities and slightly in frequencies depending on the preparation method, Cat.A contain the characteristic doublet bands about 1800 and 1700cm^{-1}, which are ascribed to the symmetric and antisymmetric vibration modes of two NO molecules coupled in the adsorbed state as dinitrosyl $(NO)_2$ structures on the same unsaturated molybdenum site[13,14]. There were varieties from Cat.A When Cat.C was exposed to NO, the band at 1828cm^{-1} increased with the NO adsorption time prolonged, and also a band at 1743cm^{-1} appeared, while after outgassing these band disappeared swift. The absence of any band at about 1800 and 1700cm^{-1} corresponding to adsorbed NO on the Cat.C indicated that there exists few proportion of sulfur vacancies which could chemisorbed NO. In light of the results from XRD (Fig3.) analysis, the possibility that the low intensity of these bands may be attributed

to a low dispersion of the MoS_2 species.

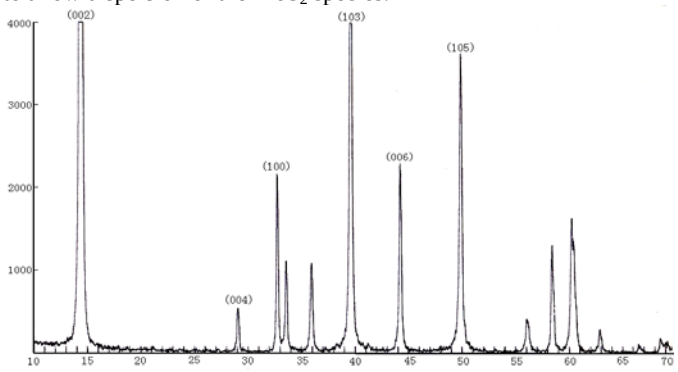

Fig3. XRD spectra of MoS_2 catalyst(Cat.C)

As expected, the spectra of NO adsorbed on Cat.B are more complex than those of Cat.A and Cat.C, when Cat.B exposed to NO, a band at 1743cm^{-1} also could be found and the band at 1828cm^{-1} raised, which is resemble to the band appeared on Cat.C. But after outgassing the spectra display bands at about 1778, 1707 and 1692cm^{-1}.The band at 1778cm^{-1} is ascribed to the symmetric vibration modes of two NO molecules coupled in the adsorbed state as dinitrosyl $(NO)_2$ structures on the same unsaturated molybdenum site, the lower frequency band at 1707 and 1692cm^{-1} correspond to antisymmetric vibration modes of dinitrosyl $(NO)_2$ species adsorbed on vacancies of sulfide molybdenum catalyst[13,14]. It is interesting to note that the band at 1778cm^{-1}, indicative of the symmetric vibrationg mode of dinitrosyl $(NO)_2$ becomes shifted about 22cm^{-1} to lower wavenumbers and the band corresponding to antisymmetric vibration modes of dinitrosyl $(NO)_2$ species appeared as two bands with respect to that of Cat.A(1800cm^{-1}). From XPS result (Fig4.), it is clear that MoS_2, MoO_2 and MoOS species exist at the surface of Cat.B, the density of electron of different species is different, so that two bands ascribed to adsorbed NO could be found located on 1707 and 1692cm^{-1}.

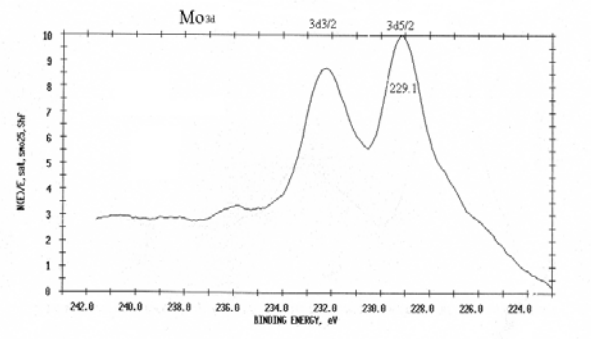

Fig4. Mo3d of XPS spectra of sulfide water-solubility Mo catalyst (Cat.B)

Form the results of our experiments, there are obvious differenced between the IR spectra of NO and thiophene adsorbed on the three catalysts above-mentioned, and the activity of thiophene hydrodesulfurization on the three catalysts show distinction to each other. Because only the unsaturated sites can adsorbed probe molecules, the surrounding of the active sites will make the spectra of adsorbed NO changed [20,21], so different absorbance peaks correlate to different active sites. On Cat.A, The doublet bands related to $(NO)_2$ structures on the same unsaturated molybdenum site [13,14] show that there exists one adsorption sites at least on the surface of sulfided Mo/Al_2O_3 catalyst. No evidence spectra of adsorbed NO on Cat.C indicated that there exists few proportion of sulfur vacancies to chemisorbed NO, a low dispersion of the MoS_2 species cannot produce adsorption sites. While NO adsorption on Cat.B shows more complex to Cat.A and Cat. C, for it was prepared at high dispersion, several unsaturated Mo sites at different chemical surrounding may exist. Comparing the intensity of the bands corresponding to adsorbed NO, it can be found that the intensity of the band on Cat.A is higher than that on Cat.B, as we all known, the intensity of adsorbed NO increased with adsorption sites on the surface of catalyst. The IR spectra of adsorbed NO suggest that the amount of the adsorption site densities decreased with the following order: sulfide $Mo/\gamma\text{-}Al_2O_3$ > sulfide water-solubility dispersed catalyst> MoS_2.

Exposure of Catalysts to Thiophene/H_2 at high temperature:

The IR spectra presented in Fig5. show that a sulfided 15wt%$Mo/\gamma\text{-}Al_2O_3$ catalyst becomes quite reactive toward thiophene when heated to 673K in the presence of thiophene/H_2, No reactivity is observed in the identical experiment for the sample of pure $\gamma\text{-}Al_2O_3$. From the result of Fig5a, the IR spectrum in the ν_{CH} region contains absorbance features at 3075, 3090 and 3109cm^{-1}, and which are ascribed to thiophene adsorbed on the surface of $\gamma\text{-}Al_2O_3$[15,16]. The IR spectrum in the ν_{CC} region shows peaks at 1400, 1408 and 1429cm^{-1}. Annealing of the catalyst at 573K for 1min leads to the production of new absorbance features in the ν_{CH} region at 2920 and 2860cm^{-1}, further annealing at 673K, the intensity of the bands at 2920 and 2860cm^{-1} increasing rapidly, these absorbance can be assigned to the ν_{CH} of CH_2 and CH_3 groups of adsorbed C_4 hydrocarbon species, the bands at 1610, 1380 and 1460cm^{-1} also could be found, the bands at 1380 and 1460cm^{-1} corresponding to δ_{CH}, while 1610 was the characteristic band of $\nu_{C=C}$[17], which confirmed that thiophene hydrogenated to C_4 hydrocarbon on Cat.A.

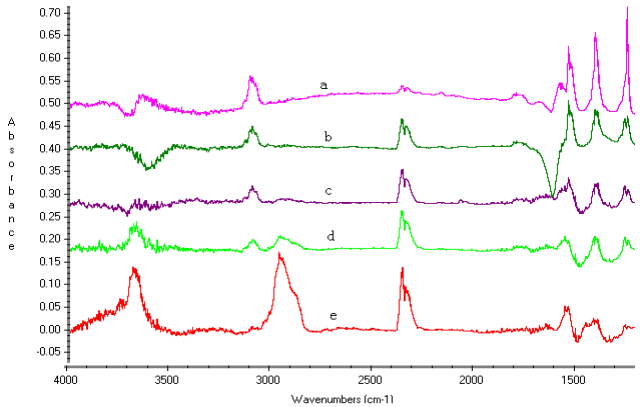

Fig5. IR spectra of adsorbed thiophene hydrogenation on Cat.A
(a) 323K; (b) 373K; (c) 473K; (d) 573K; (e) 673K

The IR spectra presented in Fig6a show that thiophene adsorbed on water-solubility dispersed molybdenum catalyst, there exist the band at 3075, 3090, 3109, 1400, 1408 and 1425cm^{-1}, which is identical to the band thiophene adsorbed on Cat.A. While new absorbance features are observed in the process of temperature increasing in the presence of thiophene/H_2, a weak and broad absorbance feature slowly develops at approximately 2640cm^{-1} which is likely due to S-H stretching vibration mode, Ratnasamy and Yerofeyev observed a similar absorbance feature in their studies of H_2 and thiophene adsorption on unsupported MoS_2 and also assigned it to an S-H stretching vibration [18,19]. Annealing at 673K, the bands at 2920, 2860, 1610 1380 and 1460cm^{-1} also could be found, which shows that thiophene can be hydrogenated to C_4 hydrocarbon on Cat.B, but the intensity of the bands corresponding to the products

produced from thiophene hydrodesulfurization lower than that on Cat.A.

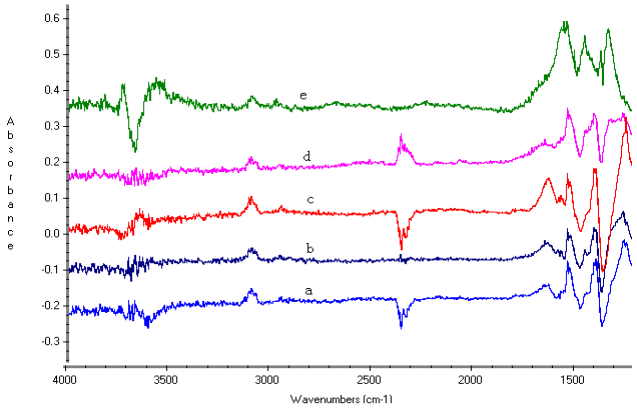

Fig6. IR spectra of adsorbed thiophene hydrogenation on Cat.B at different temperature

(a) 323K; (b) 373K; (c) 473K; (d) 573K; (e) 673K

Fig7 shows the IR spectra of thiophene adsorption and hydrodesulfurization in the presence of thiophene/H_2 on MoS_2. while thiophene adsorbed on MoS_2, there was no evidence absorbance peaks at ~1429cm^{-1}, which is ascribed to ν_{CC} of adsorbed thiophene on surface of the catalyst, after annealing at 673K in the presence of thiophene/H_2, the bands at 2920, 2860cm^{-1} could be found, but the bands corresponding to ν_{SH}, $\nu_{C=C}$ and δ_{CH} did not appeared. The results indicated that the activity of thiophene HDS on MoS_2 is lower than the above-mentioned catalyst. For MoS_2 exists as crystal, it cannot be reduced easily to produce sulfide vacancies which is the active sites for hydrodesulfurization.

As described in the results section, While H_2 and thiophene coadsorption on the three catalysts at room temperaure, a shoulder peak at 1429cm^{-1} on Cat.A and 1425cm^{-1} on Cat.B respectively appeared, which differ from the spectra of H_2 and thiophene coadsorbed on Al_2O_3, tt can be concluded that the IR spectra at ~1430cm^{-1} is caused by thiophene adsorbing on the metal center of the surface of the two catalyst. The fact that no absorbance feature is observed at ~1430cm^{-1} in the IR spectrum of Cat.C exposed to thiophene/H_2 may consistent with (a)H_2 adsorption on the sites more easily than thiophene or (b)adsoption sites cannot be produced on the surface of MoS_2 catalyst. Combined with the result of NO adsorption, it is proved that a low dispersion of the MoS_2 species cannot produce adsorption sites. The absorbance feature at ~1430cm^{-1} in the IR spectrum of thiophene adsorbed on sulfided Mo/Al_2O_3 and water-solubility dispersed molybdenum catalyst can be assigned to the symmetric ν_{CC} mode of thiophene adsorbed on MoS_2-like structures. Terbuck[22] as well as Patrick[16] also observed the same absorbance features at ~1430cm^{-1} on sulfided Mo/Al_2O_3 catalyst, and they all assign this adsorbance feature to thiophene η^1(S) bonded to cus $Mo^{\delta+}$ sites of MoS_2-like structures of the sulfided Mo catalyst. The peak position of this ν_{CC} mode is shifted to higher wavenumbers than is observed for liquid thiophene(1406cm^{-1}), it is well known that the vibrational frequencies of ring stretching modes of the heterocyclic aromatic molecules are sensitive to their bonding environment on a catalyst surface. The symmetric ν_{CC} mode of should be shifted to higher wavenumbers when thiophene is adsorbed on a metal center via its sulfur atom and should be shifted to lower wavenumbers when thiophene is π-bonded to a metal center, the fact that the peak position of the ν_{CC} mode shifts to higher wavenumbers when thiophene adsorbed on sulfided Mo/Al_2O_3 and water-solubility catalysts provides the evidence that thiophene is coordinated via its sulfur atom to cus Mo sites on the catalyst surface. Since the adsorbed species associated with the adsorbance features in the region of 2800-3000cm^{-1} region are believed to be thiophene hydrodesulfurized C_4 hydrocarbon fragments, Compared the spectra of different catalyst after annealing in the presence of thiophene and H_2 at 673K for the same time, it could be concluded that the trend in thiophene reactivity is observed to be the following: sulfide Mo/γ-Al_2O_3 > sulfide water-solubility dispersed catalyst> MoS_2. The observed trend of the reactivity of thiophene hydrodesulfurization reflects the catalyst activity strongly correlates to the dispersion status, high dispersion is propitious to improving the activity of the catalyst.

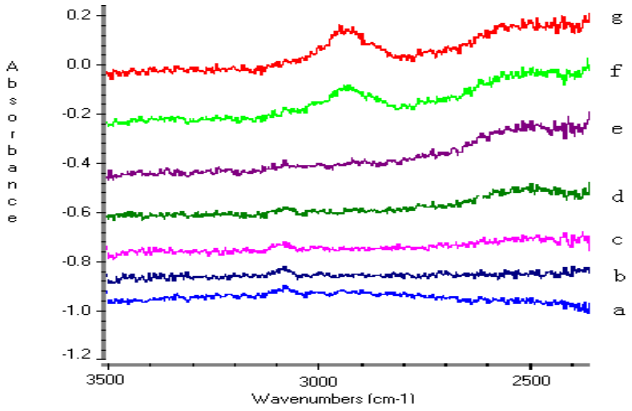

Fig7. IR spectra of adsorbed thiophene hydrogenation onCat.C at different temperature(a) 323K; (b) 373K; (c) 473K; (d) 573K; (e) 673K (f) after 30min under 0.04MPa H_2/thiophene at673K; (g) 1h under 0.04MPa H_2/thiophene at 673K;

Conclusion

The adsorption and reaction of thiophene on the surface of the sulfided molybdenum catalysts in the presence of hydrogen have been studied by FT-IR spectroscopy combined with NO adsorption. The IR spectra of adsorbed NO suggest that the amount of the adsorption site densities decreased with the following order: sulfide Mo/γ-Al_2O_3 > sulfide water-solubility dispersed catalyst> MoS_2. Thiophene is weakly chemisorbed to the sites located on MoS_2-like structures and on uncovered alumina regions of sulfide molybdenum catalyst. Based upon interpretation of IR spectra, the adsorption mode of thiophene on sulfide Mo portion of the catalyst surface has been determined to be η^1(s). Thiophene is observed to become reactive on sulfided Mo catalysts in the presence of gas-phase hydrogen and at high temperatures. Thiophene hydrodesulfurization(HDS) activities of several sulfided Mo catalysts decreasing in the following order: sulfide Mo/γ-Al_2O_3 > sulfide water-solubility dispersed catalyst> MoS_2, which are consistent to the adsorption site densities.

REFERRENCES

(1) Diemann, E., Weber, T., Muller, A. J. Catal. 1994,148:288
(2) Ratnasamy, P., Fripiat, J. J., J. Chem. Soc., Faraday Trans. 1970,66:2897
(3) Dong, L., Duckett, S. B., Ohman, K. F. et al. J. Am. Chem. Soc.1992, 114:151
(4) Luo, S., Rauchfuss, T. B., Gan, Z. J. Am. Chem. Soc, 1993, 115:4943
(5) Mitchell P C H, Green D A, Grimblot J et al. J. Bull. Soc. Chim. Belg. 1995,104:325
(6) Oyama, S. T., Catal. Today, 1992,15:179

(7) Lee, J. S., Lee, K. H. and Lee, J. Y., J Phys. Chem. 1992,96:362
(8) Tauster, S. J., Pecoraro, T. A., and Chianelli, R. R. J. Catal. 1980,63:515
(9) Bachelier, J., Tilliette, M. J., Duchet, J. C. et al. J. Catal. 1982, 76:300
(10) Bachelier, J., Duchet, J. C., Cornet, D. Bull. Soc. Chim. Belg. 1981,90:1301
(11) Muller, B., van Langeveld, A., D, Moulijn, J. A. et al. J. Phys. Chem. 1993, 97:9028
(12) Xue Kong, Dong Liu, Zongxian Wang et al. Prepr. Pap. ACS Div, Pet. Chem. 2003,48:265
(13) Yasuaki O, Yukihiro K, Yoshiyuki M. J. Catal. 1981,70:445
(14) Topsoe N Y, Topsoe H. J Catal, 1982,75:354
(15) Zili, W., Yongjun, C., Shuwu, Y., J. Catal. 2000,194:23
(16) Patrick M, Diana C P, Brian P W et al. J. Phys. Chem. B 2000, 104:3237
(17) Little L H. Infrared Spectra of Adsorbed Species[M]. London: Academic Press,1966
(18) Yerofeyev V I, Kaletchits I V. J Catal. 1984,86:55
(19) Ratnasamy, P., Fripiat, J. J. J. Chem. Soc. Faraday Trans. 1970, 66:2897
(20) Goldwasser, J., Fang, S. M., Houalla, M., et al. J. Catal.1989,115:34
(21) Redey, A., Goldwasser, J., Hall, W. K. J. Catal. 1988,113:82
(22) Tarbuck T L, Mccrea K M, Logan J W et al. J. Phys. Chem. 1998,102:7845